

## ABSTRACT

KISHORE, PINAK. An Antenna-Independent Approach to the Capacity of a Wireless System. (Under the direction of Professor Brian L. Hughes.)

Information theory (IT) promises a huge increase in capacity for systems equipped with multiple antennas at both the transmitter and receiver (called Multiple-Input Multiple-Output or MIMO) in a rich multipath scattering environment relative to single antenna systems (called Single-Input Single-Output or SISO). Since the first results on capacities for MIMO systems were published by Telatar [2] and Foschini *et al.* [3], there has been an extensive research effort to develop techniques and algorithms to realize the gains promised by MIMO systems. Most of these studies have focussed on particular antenna systems such as uniform linear arrays and have derived channel capacities using a statistical signal-space approach under ideal fading conditions. The number and locations of the antennas in such systems, however constrains the information that is extracted from the underlying electromagnetic field thereby giving antenna-dependent capacity results. To overcome these constrains imposed by particular antenna systems and to find the true capacity of systems limited only by their volume, we need to look at continuous-time systems in an antenna-independent way. In this thesis, we look at one such system which consists of a spherical volume at the transmitter having some arbitrary current distribution and radiating an electric field around it. The receiver consists of a spherical shell

located in the far-field of the transmitter capturing all the signals radiated by it. We then use electromagnetic theory to derive the input-output equation for this system and use an orthonormal series expansion to reduce it to the form of a MIMO channel. We then calculate the capacity and the spatial degrees of freedom for such a system and look at how they vary with the size of the transmitting volume and the available transmitter power. We show that the spatial degrees of freedom grow linearly with the effective aperture of the spherical volume and the capacity grows even faster. We also investigate the increase in spatial degrees of freedom and capacity that can be achieved by using three-dimensional (tri-polarized) current distributions at the transmitter instead of one-dimensional (uni-polarized) current distributions. We show that capacity gains of 3 times can be achieved for a sufficiently large transmitter. Lastly, we look at a more realistic complete transmit-receive system with an identical spherical volume at the receiver and an ideal fully-scattered channel connecting the transmitter to the receiver. We model the channel as a Rayleigh fading channel and compare the results on capacity and spatial degrees of freedom with previous results.

**An Antenna-Independent Approach to the Capacity of a Wireless System**

by

**Pinak Kishore**

A thesis submitted to the Graduate Faculty of  
North Carolina State University  
in partial fulfillment of the  
requirements for the Degree of  
Master of Science

**Department of Electrical and Computer Engineering**

Raleigh

August 12, 2005

**Approved By:**

---

Dr. Huaiyu Dai

---

Dr. Gianluca Lazzi

---

Dr. Brian L. Hughes  
Chair of Advisory Committee

To my parents and my sisters ...

## Biography

Pinak Kishore was born in Punjab, India on July 15, 1979. He received his B.E. degree in Electronics and Communication Engineering in 2001 from Netaji Subhas Institute of Technology (formerly DIT), Delhi University, India. He then joined the Embedded Systems Group of Infosys Technologies Ltd. in Bangalore, India and worked there for about one and a half years. Later in the summer of 2003, he worked as a project assistant in the signal processing division at the Indian Institute of Sciences (IISc), Bangalore under the guidance of Dr. K.V.S. Hari. In the fall of 2003, he started his Master of Science degree study at the North Carolina State University, Raleigh. He started working on his thesis in the fall of 2004 under the guidance of Dr. Brian L. Hughes and is currently working towards its completion.

## Acknowledgements

First, I would like to sincerely thank my advisor, Dr. Brian L. Hughes for giving me an opportunity to work in his research group and funding my study at NCSU. His support and guidance is instrumental in the successful completion of this thesis. His enthusiasm towards the subject and his intuitive way of approaching problems have been constant motivating factors for me. I also thank Dr. Gianluca Lazzi and Dr. Huaiyu Dai for being on my thesis committee and providing valuable feedback and suggestions on this thesis.

I am immensely thankful to Sandeep Krishnamurthy for all the help he has provided throughout my thesis. He has literally guided me through my thesis with his technical expertise on the subject.

I also extend my thanks to other members of the research group including Chris Mary James, Pallav Sudarshan, Ajith Kamath, Xinying Yu and Mahmud Jalnase who were always willing to help me out. A special thanks is due to my friend Anu Chaudhary who has been always there for me with her support.

Finally, I express my deepest gratitude to my parents and sisters for their unconditional love and unflinching support. I thank them for always believing in me and encouraging me to do whatever I believed in. But for them, I would not have reached this far today.

# Contents

<b>List of Tables</b>	<b>vii</b>
<b>List of Figures</b>	<b>viii</b>
<b>1 Introduction</b>	<b>1</b>
<b>2 Background and Signal Model</b>	<b>8</b>
2.1 MIMO System Model . . . . .	9
2.1.1 Channel Capacity for a MIMO System . . . . .	10
2.2 Signal Model for the Continuous-Time System . . . . .	16
<b>3 A Discrete-Time Equivalent System and its Analysis</b>	<b>20</b>
3.1 An Orthonormal Basis for the Electric Field . . . . .	22
3.1.1 3-d Current Distributions . . . . .	22
3.1.2 1-d Current Distributions . . . . .	30
3.2 Normalization and Capacity Calculations . . . . .	31
3.2.1 Signal-to-Noise Ratio . . . . .	31

3.2.2	Normalization . . . . .	32
3.2.3	Capacity Calculations for Our System . . . . .	33
3.3	Spatial Degrees of Freedom . . . . .	36
3.4	Complete Transmit-Receive System . . . . .	39
3.4.1	Capacity Calculations and Normalization for the Complete Sys- tem . . . . .	42
<b>4</b>	<b>Simulation Results</b>	<b>44</b>
4.1	Error Due to System Truncation . . . . .	45
4.2	Spatial Degrees of Freedom . . . . .	49
4.3	Channel Capacity . . . . .	52
4.4	Increase in Capacity and Spatial Degrees of Freedom on using 3-d Current Distributions . . . . .	57
4.5	Impact of Truncation on Capacity . . . . .	59
4.6	Results for the Complete Transmit-Receive System . . . . .	62
<b>5</b>	<b>Conclusions</b>	<b>69</b>
	<b>Appendices</b>	<b>71</b>
	<b>A Recurrence Relations for Spherical Harmonics</b>	<b>72</b>
	<b>B Impact of Truncation Errors on the Capacity Calculation</b>	<b>77</b>
	<b>Bibliography</b>	<b>82</b>

# List of Tables

4.1	Ratio $n^*(1-d)/4\pi^2a^2$ for different SNR values and radius of the spherical volume . . . . .	50
4.2	Spatial Degrees of Freedom $n^*(1-d)$ for different SNR values and radius of the spherical volume . . . . .	52

# List of Figures

2.1	$N_r \times N_t$ MIMO system . . . . .	10
2.2	Water-pouring in space . . . . .	15
2.3	Signal Model . . . . .	17
3.1	Complete Signal Model with Transmitter, Receiver and Channel . . . .	40
4.1	First 1000 eigenvalues for systems truncated to lengths of 1875 and 2700 respectively, and radius $a = 1$ . . . . .	46
4.2	First 1000 eigenvalues for systems truncated to lengths of 1875 and 2700 respectively, and radius $a = 3$ . . . . .	47
4.3	Difference in eigenvalues for systems truncated to lengths of 1875 and 2700, and radius $a$ varying from 0.5 to 3 . . . . .	48
4.4	Plot of $n^*(3\text{-d})$ vs. $4\pi^2 a^2$ at SNR's of 20 dB and 0 dB respectively . .	50
4.5	Plot of $n^*(1\text{-d})$ vs. $4\pi^2 a^2$ at SNR's of 20 dB and 0 dB respectively . .	51
4.6	Capacities vs. SNR for 3-d input current distributions and $a$ varying from 0.5 to 3 . . . . .	53

4.7	Capacities vs. SNR for 1-d input current distributions with $a$ varying from 0.5 to 3 . . . . .	54
4.8	Capacity/Dimension vs. SNR for 3-d input current distributions with $a$ varying from 0.5 to 3 . . . . .	55
4.9	Capacity vs. $4\pi^2a^2$ with SNR varying from 0 dB to 20 dB . . . . .	56
4.10	Capacity Ratio $C(3-d)/C(1-d)$ vs. $a$ for SNR's of 0db and 20db respectively . . . . .	58
4.11	Ratio $n^*(3-d)/n^*(1-d)$ vs. $a$ for SNR's of 0 dB and 20 dB respectively	60
4.12	Capacity bounds and calculated capacity vs. SNR for $a = 3$ . . . . .	61
4.13	Plot of $n^*(3-d)$ vs. $4\pi^2a^2$ for the complete system at SNR's of 20 dB and 0 dB respectively . . . . .	63
4.14	Plot of $n^*(1-d)$ vs. $4\pi^2a^2$ for the complete system at SNR's of 20 dB and 0 dB respectively . . . . .	64
4.15	Capacities vs. SNR for the complete system with 3-d input current distributions and $a$ varying from 0.5 to 3 . . . . .	65
4.16	Capacities vs. SNR for the complete system with 1-d input current distributions and $a$ varying from 0.5 to 3 . . . . .	66
4.17	Capacity vs. $4\pi^2a^2$ for the complete system and SNR varying from 0 dB to 20 dB . . . . .	67
4.18	Capacity Ratio $C(3-d)/C(1-d)$ vs. $a$ for the complete system at SNR's 0db and 20db respectively . . . . .	68

# Chapter 1

## Introduction

Claude E. Shannon [1] laid the foundations of Information Theory (IT) in his seminal paper ‘A Mathematical Theory of Communications’ in 1948 which gives fundamental limits on the performance of communication systems. IT gives the maximum rate at which reliable communications is possible for a given channel, which is called the channel capacity. Through technological advances and extensive research in the area of coding theory over the years, researchers have been able to design communication systems which perform within a fraction of a dB of Shannon’s capacity limit for Additive White Gaussian Noise (AWGN) wireless channels [5]. However, the demand for data rate over wireless systems has increased at such a pace, that even optimal single-antenna systems ( called Single-Input Single-Output or SISO) have been unable to keep up with it. The limited amount of radio spectrum restricts the

data rates that we can achieve over SISO channels, which has motivated researchers to look at other ways of increasing the data rate without increasing the spectrum usage.

This research led to the discovery in the late 90's of wireless communication systems equipped with multiple antennas at both the transmitter and receiver (called Multiple-Input Multiple-Output or MIMO) that can achieve huge capacity gains over conventional SISO systems in a rich multipath scattering environment. Telatar in [2] and Foschini *et al.* in [3] gave the first results on the capacities of MIMO wireless systems and showed that, under the assumptions of an ideal Rayleigh fading channel, capacity scales linearly with the minimum of the number of antennas at the transmitter and the receiver. Because of the phenomenal promise of MIMO systems in increasing data rates without using any extra bandwidth, it has emerged as one of the most significant technical breakthroughs in modern communications. Such has been the impact of MIMO technology, that in just a few years after its invention the technology has started to be incorporated into major commercial wireless standards such as broadband wireless access systems, wireless local area networks (WLAN) and third-generation (3G) networks.

MIMO systems can be defined simply as wireless communication systems which are equipped with multiple-antenna elements at the transmitter as well as the receiver. A core idea in MIMO systems is *space-time* signal processing in which time (the natural dimension of digital communication data) is complemented with the spa-

tial dimension inherent in the use of multiple spatially-distributed antennas. A key feature of MIMO systems is the ability to turn multipath propagation, traditionally a pitfall of wireless transmission, into a benefit for the user. MIMO effectively takes advantage of random fading [2, 3, 4] to multiply transfer rates. At high signal-to-noise ratios (SNR's), capacity actually increases linearly with the number of spatial degrees of freedom. For the case of a MIMO system under independent and identically distributed (i.i.d) fading conditions, the spatial degrees of freedom are equal to the minimum of the number of antennas at the transmitter and the receiver and therefore the capacity for such systems scales linearly with the number of antennas. This capacity increase, however, requires a scattering environment such that the channel gain matrix is full rank and has independent entries. The channel matrix has random entries corresponding to different channel realizations with each entry representing the channel gain between a transmit-receive antenna pair for a particular channel realization. Linear growth of capacity also requires perfect estimates of the channel gain matrix at the receiver. Perfect estimates of the channel matrix at the transmitter as well only increases the constant multiplier associated with linear scaling of capacity [6].

The prospect of many orders of magnitude improvement in wireless communication performance at no cost of extra spectrum (only hardware and complexity is added) has resulted in an extensive research effort to develop techniques and algorithms to realize the gains promised by MIMO systems. The research effort has re-

sulted in substantial progress in areas as diverse as channel modelling, signal processing and coding theory specifically targeting multiple-antenna systems (Space-Time Codes or STC), antenna design and multiple-antenna-aware cellular design. An excellent summary of the current state of affairs in MIMO research has been provided by Gesbert *et al.* in [6] and Goldsmith *et al.* in [7].

Most of the prior studies of MIMO systems have focussed on particular antenna systems such as uniform linear arrays and have derived channel capacities using a statistical signal-space approach under ideal fading conditions. It is not clear, however, whether uniform linear arrays extract all of the useful information from the underlying electromagnetic field. It is therefore natural to ask whether capacity would be increased by observing the entire electromagnetic field within the aperture of the array. Recently, Poon *et al.* in [8] have considered the number of spatial degrees of freedom available in a wireless system in which the transmitter and receiver capture (or generate) an arbitrary current distribution within a given volume. Using some heuristic methods, they argue that the number of spatial degrees of freedom tends to a deterministic limit for a given propagation environment and physical constraints of size and geometry at the antenna arrays. [10, 11, 12, 13] are a few other papers which have looked at systems constrained only by the size of the transmitter and the receiver.

In this thesis, we use numerical methods and an antenna-independent approach to investigate the capacity and number of spatial degrees of freedom available in a

wireless system in which the transmitter and receiver generate (or capture) the entire current distribution within a given aperture. The system that we consider consists of a spherical volume at the transmitter having some arbitrary current distributions and radiating an electric field into the surrounding space. The receiver consists of a spherical shell located in the far-field of the transmitter. In any realistic propagation environment, of course, the receiver will observe only samples of the transmitter's far-field signal, corresponding to the locations of the significant scatterers. Since our aim here is to understand the limitations imposed by the physical dimensions of the transmitter, however, we will adopt the optimistic model of an all-powerful receiver that is able to collect all the signals radiated by the transmitter in the far-field. We use electromagnetic theory to derive the continuous-time input-output equation for this channel and later use an orthonormal series expansion to reduce it to an equivalent MIMO channel. We consider the spherical volume as a continuous array, which is composed of an infinite number of antennas separated by infinitesimal distances. This eliminates the need to specify *a priori* the number of antennas and their relative positions on the antenna arrays. The spherical volume is constrained to have radius  $a$ <sup>1</sup> making its effective aperture<sup>2</sup>  $\mathcal{A}$  equal to  $\pi a^2$ . We assume the receiver observes all far-field signals, so that the solid angle  $|\Omega|$  corresponding to the angular spread is equal to  $4\pi$ . We show using numerical simulations that for such a system the spatial

---

<sup>1</sup>Radius  $a$  is in terms of the wavelength  $\lambda$  of the sinusoidal electromagnetic field, explained further in Section 2.2

<sup>2</sup>The effective aperture of an antenna is its capture area. For a receiving antenna it is the frontal area from which the antenna extracts energy from passing electromagnetic waves.

degrees of freedom increase linearly with the effective aperture  $\mathcal{A}$  of the spherical volume and the capacity increases at an even faster rate. We further investigate the gain in capacity and spatial degrees of freedom that can be achieved by using three-dimensional (3-d) current distributions in the antennas instead of one-dimensional (1-d) current distributions. We again use numerical simulations to show that capacity gains upto a factor of 3 can be achieved for a sufficiently large transmitter, with the gain factor being between 2-2.8 for practically-sized spherical arrays having a radius of a few wavelengths.

Finally we consider a more realistic complete transmit-receive system consisting of the conducting spherical volume at the transmitter, an identical conducting spherical volume at the receiver and a Rayleigh fading channel matrix connecting the two. We again use electromagnetic theory to study the system and numerical simulations to compute the capacity and spatial degrees of freedom for the system. Comparison of results with the previous system show that the trends in capacity values and spatial degrees of freedom observed by the previous system are also followed by this more realistic complete transmit-receive system. Although our choice of a fully scattered environment and an ideal Rayleigh fading channel for the complete system is a simplifying assumption which does not always hold true in practice, we point to [9] which provides a detailed analysis of the impact of various practical scattering environments on channel capacity for linear arrays.

The rest of this thesis is organized as follows. In Chapter 2, we start by review-

ing the mathematical model and the capacity derivations for MIMO systems based on IT. These results are used later to compute capacities for the continuous-time system considered in this thesis. Later in the chapter, we describe the signal model for the continuous-time system and also derive an input-output relation for it using electromagnetic theory.

In Chapter 3, we start by reducing the continuous-time system model to a discrete-time equivalent to ease the analysis and numerical simulations for the system. An orthonormal series expansion is used for system reduction and to derive the discrete-time input-output expressions for the system. Using these expressions and an appropriate normalization, we give the capacity formulas for the system. We also model a complete transmit-receive system by introducing the channel scattering matrix and an identical spherical volume at the receiver.

In Chapter 4, we present the results of numerical simulations. Results on the eigenvalues, spatial degrees of freedom and capacities of the systems outlined in Chapter 3 are detailed and analyzed.

Finally, in Chapter 5, we summarize our conclusions and offer some possible research directions for the future.

## Chapter 2

# Background and Signal Model

In this chapter, we first give a background on MIMO systems and review their mathematical models. We then review the definition and derivations of channel capacity for MIMO systems based on IT. Later, we introduce a model of a wireless system in which a transmitting spherical volume communicates with a receiving spherical shell located in the far-field of the transmitter. We also derive a continuous-time input-output relation for this system using electromagnetic theory in this chapter.

The following notation will be used in this thesis. Bold uppercase letters ( $\mathbf{H}, \mathbf{C}, \dots$ ) used in discrete-time equations represent matrices, whereas bold uppercase letters used in continuous-time equations ( $\mathbf{E}(\mathbf{r}), \mathbf{J}(\mathbf{r}'), \dots$ ) represent vector-valued functions. Similarly, bold lowercase letters ( $\mathbf{y}, \mathbf{x}, \dots$ ) in discrete-time equations represent column vectors and bold lowercase letters in continuous-time equations ( $\mathbf{r}, \mathbf{r}', \dots$ ) represent

location vectors.  $\mathcal{E}(\mathbf{x})$  represents the expectation of random vector  $\mathbf{x}$ .  $\mathbf{A}^T$ ,  $\mathbf{A}^\dagger$  and  $\text{Tr}(\mathbf{A})$  represent the transpose, conjugate transpose and trace of matrix  $\mathbf{A}$ , respectively. Lowercase  $i$  denotes the square root of  $-1$ .  $\mathbf{I}_k$  denotes the identity matrix of size  $k$ . The notation  $\mathbf{n} \sim \mathcal{CN}(\bar{\mathbf{n}}, \Sigma_{\mathbf{n}})$  indicates that  $\mathbf{n}$  is a complex Gaussian distributed random vector with mean  $\bar{\mathbf{n}}$  and covariance matrix  $\Sigma_{\mathbf{n}}$ . The curl operator with respect to  $\mathbf{r}$  is represented by  $\nabla_{\mathbf{r}} \times$ .

## 2.1 MIMO System Model

MIMO systems are wireless communication systems which are equipped with multiple antennas at the transmitter as well as the receiver. Fig. 2.1 shows an  $N_r \times N_t$  MIMO system with  $N_t$  antennas at the transmitter and  $N_r$  antennas at the receiver. The signal that arrives at each of the  $N_r$  receive antennas is a superposition of the  $N_t$  faded transmitted signals and noise. The use of multiple antennas at the transmitter and the receiver thus provides a matrix channel to transmit data, where the entries of the matrix give the complex fading path gain across various transmit-receive antenna pairs. Since the fading conditions are random, the entries of the channel matrix are also random with each outcome corresponding to a particular channel realization. The probability distribution of these matrix entries depend on the fading characteristics of the channel and are a crucial factor determining the performance of MIMO systems.

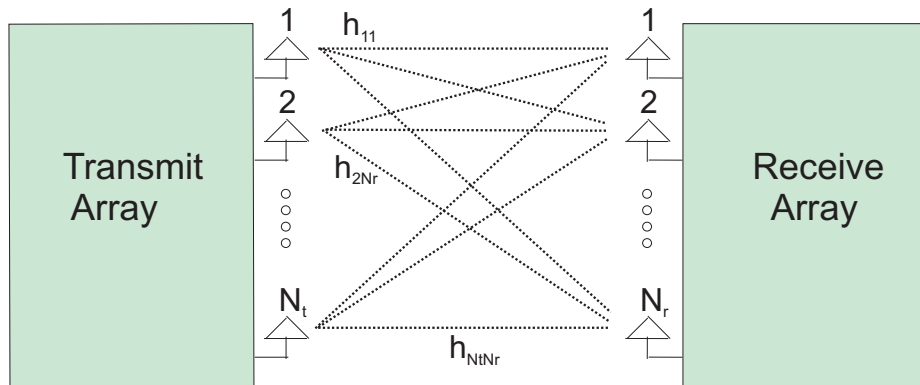


Figure 2.1:  $N_r \times N_t$  MIMO system

### 2.1.1 Channel Capacity for a MIMO System

Channel capacity is defined as the maximum rate at which information can be sent over the channel with an arbitrarily low probability of error. In the information-theoretic sense, it is the maximum mutual information between the channel input and the channel output. Here we review the derivations for channel capacity of the MIMO system defined above. These capacity formulas for MIMO systems were first derived by Telatar and Foschini *et al.* independently in [2] and [3], respectively.

Before proceeding with capacity calculations, we state the underlying assumptions for this system model. We assume that the delay spread of the multipath is small, i.e. we have a frequency-flat fading scenario. We also assume slow fading conditions, i.e. the symbol time is small compared to the coherence time of the channel. The antennas at the transmit and receive arrays are assumed to be spaced so as to produce

independent fading between each transmit-receive antenna pair. The individual path gains and the noise variables are therefore independent and identically distributed (i.i.d.) and are assumed to have a complex Gaussian distribution. The total average transmit power available at the transmitter is  $P$ .

Denoting the  $N_r \times N_t$  channel matrix by  $\mathbf{H}$ , the input-output relation for the MIMO system can be written [14, pp. 63] as

$$\mathbf{y} = \sqrt{\frac{P}{N_t}} \mathbf{H} \mathbf{x} + \mathbf{n} \quad (2.1)$$

where  $\mathbf{y}$  is the  $N_r \times 1$  received signal vector,  $\mathbf{x}$  is the  $N_t \times 1$  transmitted signal vector,  $\mathbf{n}$  is  $\mathcal{CN}(\mathbf{0}, \mathbf{I}_{N_r})$ , i.e. all components of the noise vector are complex Gaussian distributed and have a zero mean and unit variance. In order to constrain the total average power transmitted over a symbol period the covariance matrix of  $\mathbf{x}$ ,  $\mathbf{Q} = \mathcal{E}\{\mathbf{x}\mathbf{x}^\dagger\}$  must satisfy  $\text{Tr}(\mathbf{Q}) = N_t$ .

Using the information-theoretic definition of capacity being equal to maximum mutual information between the input and output vectors  $\mathbf{x}, \mathbf{y}$ , we have for the MIMO system

$$C = \max_{\text{Tr}(\mathbf{Q})=N_t} \mathbf{I}(\mathbf{x}, \mathbf{y}) \quad (2.2)$$

where the maximization is performed over the distribution of input vector  $\mathbf{x}$  subject to the power constraint. It can be shown that the input distribution that maximizes mutual information for a given power constraint is Gaussian [2].

Since the channel matrix  $\mathbf{H}$  is random, the information rate in (2.2) is also a random

variable taking on different values for different channel realizations. In analyzing the capacity of fading channels, two commonly-used statistics are the ergodic capacity (also called Shannon Capacity) and the outage capacity [14]. The ergodic capacity is calculated by taking the ensemble average of the maximum information rate over all channel realizations. Outage capacity analysis quantifies the level of performance that is guaranteed with a certain level of reliability. For e.g.,  $q\%$  outage capacity is defined as the information rate that is guaranteed for  $(100 - q)\%$  of the channel realizations. We will consider only the notion of ergodic capacity in this thesis.

Rewriting (2.2) in terms of the ergodic capacity, we have

$$C = \max_{\text{Tr}(\mathbf{Q})=N_t} \mathcal{E}[\mathbf{I}(\mathbf{x}, \mathbf{y})] \quad (2.3)$$

which on substitution of  $\mathbf{x}$  and  $\mathbf{y}$  easily reduces to

$$C = \max_{\text{Tr}(\mathbf{Q})=N_t} \mathcal{E} \left[ \log_2 \det \left( \mathbf{I}_{N_r} + \frac{P}{N_t} \mathbf{H} \mathbf{Q} \mathbf{H}^\dagger \right) \right] \text{ bps/Hz.} \quad (2.4)$$

Now we look at two different cases for capacity calculations. In the first case, the transmitter does not have the complete channel state information (NCSI case), while in the second case the transmitter has complete channel state information (CSI case).

In both the cases, the receiver is assumed to have complete CSI.

### NCSI Case

If the transmitter has no information about the channel, then under Rayleigh fading conditions, i.e.  $\mathbf{H}$  is  $\mathcal{CN}(\mathbf{0}, \mathbf{I}_{N_t})$ , the input vector  $\mathbf{x}$  may be chosen to be

non-preferential, i.e.  $\mathbf{Q} = \mathbf{I}_{N_t}$ . This implies that all the transmit antennas send independent and equal-power signals. Therefore, the capacity (2.4) for this case becomes

$$C = \mathcal{E} \left[ \log_2 \det \left( \mathbf{I}_{N_r} + \frac{P}{N_t} \mathbf{H} \mathbf{H}^\dagger \right) \right] \text{ bps/Hz.} \quad (2.5)$$

which easily reduces to

$$C = \mathcal{E} \left[ \sum_{i=1}^r \log_2 \left( 1 + \frac{P}{N_t} \lambda_i \right) \right] \quad (2.6)$$

where  $r$  is the rank of  $\mathbf{H}$  and  $(\lambda_1, \dots, \lambda_r)$  are the positive eigenvalues of  $\mathbf{H} \mathbf{H}^\dagger$ .

### CSI Case

In the NCSI case we saw that equal-power allocation was a logical scheme to adopt since the transmitter had no information about the channel. However, for the CSI case, when the transmitter has knowledge about the channel, the capacity is increased by employing a different strategy for power allocation. It has been shown in [2] and [3] that, in the case when channel is known to the transmitter, the individual channel modes may be accessed through linear processing at the transmitter and receiver. Let the input signal vector  $\tilde{\mathbf{x}}$  be  $\mathcal{CN}(\mathbf{0}, \mathbf{I}_{N_t})$ . By the singular value decomposition theorem,  $\mathbf{H}$  can be written as  $\mathbf{H} = \mathbf{U} \mathbf{D} \mathbf{V}^\dagger$ , where  $\mathbf{U}$  and  $\mathbf{V}$  are unitary matrices and  $\mathbf{D}$  is a  $r \times r$  diagonal matrix with  $(\sqrt{\lambda_1}, \dots, \sqrt{\lambda_r})$  along the diagonal. If we pre-multiply the input vector  $\tilde{\mathbf{x}}$  by  $\mathbf{V}$  prior to transmission and pre-multiply the received

signal vector  $\mathbf{y}$  by  $\mathbf{U}^\dagger$ , then the effective input-output relation for the system becomes

$$\begin{aligned}\tilde{\mathbf{y}} &= \sqrt{\frac{P}{N_t}} \mathbf{U}^\dagger \mathbf{H} \mathbf{V} \tilde{\mathbf{x}} + \mathbf{U}^\dagger \mathbf{n} \\ &= \sqrt{\frac{P}{N_t}} \mathbf{D} \tilde{\mathbf{x}} + \tilde{\mathbf{n}}\end{aligned}\quad (2.7)$$

where  $\tilde{\mathbf{x}} = \mathbf{V}^\dagger \mathbf{x}$ ,  $\tilde{\mathbf{y}} = \mathbf{U}^\dagger \mathbf{y}$  and  $\tilde{\mathbf{n}}$  is the transformed noise vector with covariance matrix  $\mathcal{E}(\tilde{\mathbf{n}}\tilde{\mathbf{n}}^\dagger) = \mathbf{I}_r$ . The vector  $\tilde{\mathbf{x}}$  must satisfy the power constraint  $\text{Tr } \mathcal{E}(\tilde{\mathbf{x}}\tilde{\mathbf{x}}^\dagger) = N_t$ .

The expression above shows that, with channel knowledge at the transmitter,  $\mathbf{H}$  can be explicitly decomposed into parallel SISO channels

$$\tilde{y}_i = \sqrt{\frac{P}{N_t}} \sqrt{\lambda_i} \tilde{x}_i + \tilde{n}_i \quad i = 1, 2, \dots, r \quad (2.8)$$

The capacity of such a system is the sum of the capacities of the individual SISO channels and can be written as

$$C = \max_{\sum P_i = N_t} \mathcal{E} \left[ \sum_{i=1}^r \log_2 \left( 1 + \frac{P P_i}{N_t} \lambda_i \right) \right] \quad (2.9)$$

where  $P_i = \mathcal{E}\{|\tilde{x}_i|^2\}$  is the transmit energy in the  $i$ th sub-channel and the maximization is performed over the power distribution  $(P_1, \dots, P_r)$  subject to the total power constraint  $\sum P_i = N_t$ . From (2.9), it is easily seen that the optimal power allocation is the well-known water-pouring distribution [15, pp. 252]. The optimum power distributions  $P_i^{opt}$  satisfy

$$P_i^{opt} = \left( \mu - \frac{N_t}{P \lambda_i} \right)^+ \quad i = 1, \dots, r \quad (2.10)$$

where  $\mu$  is a constant satisfying the power constraint

$$\sum_{i=1}^r P_i^{opt} = \sum_{i=1}^r \left( \mu - \frac{N_t}{P \lambda_i} \right)^+ = N_t \quad (2.11)$$

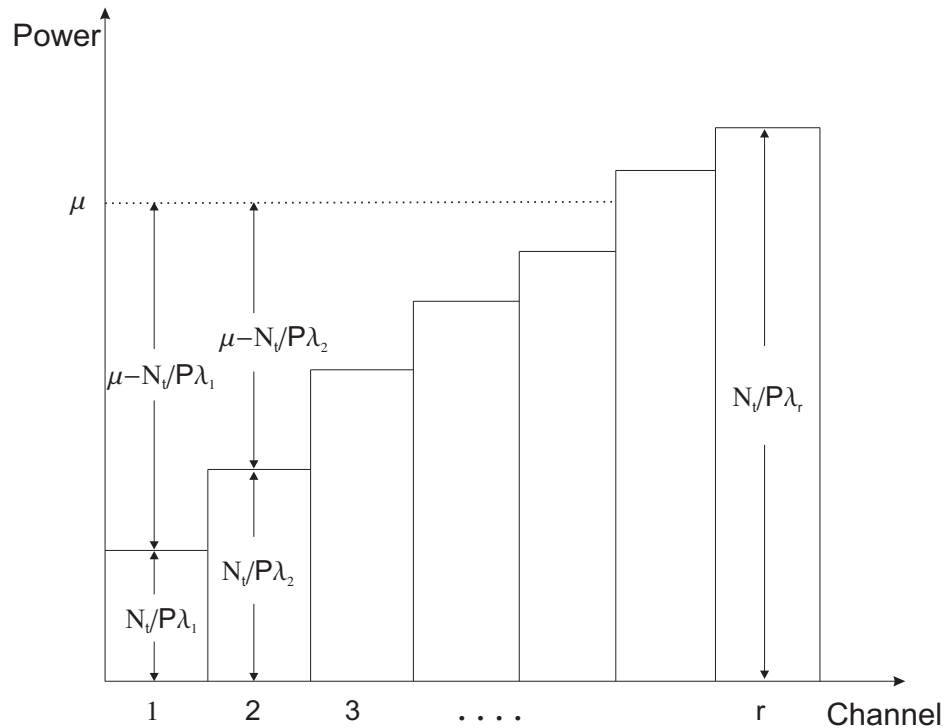


Figure 2.2: Water-pouring in space

and  $(x)^+$  is given by

$$(x)^+ = \begin{cases} x, & \text{if } x \geq 0 \\ 0, & \text{if } x < 0 \end{cases} \quad (2.12)$$

The water-pouring scheme is illustrated in Fig. 2.2. The scheme can be interpreted as pouring a volume  $N_t$  of water into a tank with blocks equal to  $N_t/P$  times the inverse of eigenvalues  $(\lambda_1, \dots, \lambda_r)$ . Substituting for  $P_i^{opt}$  in (2.9), we obtain

$$C = \mathcal{E} \left[ \sum_{i:(P\lambda_i/N_t)^{-1} \leq \mu} \log_2 \left( \mu \frac{P}{N_t} \lambda_i \right) \right] \quad (2.13)$$

## 2.2 Signal Model for the Continuous-Time System

The current distributions generated in the antenna elements and the electric fields due to it are continuous-time electromagnetic quantities. Multiple-antenna systems like the one discussed in the previous section have the effect of sampling the electromagnetic field at the location of the antennas. A particular antenna system having a certain number of antennas at specific locations would therefore restrict the amount of information that is extracted from the electromagnetic field. To overcome this restriction placed by the number and locations of the antennas, and to find the maximum information-exchange possible between the transmitter and the receiver from the electromagnetic field, we need to look at a continuous-time system. By studying one such system in this thesis, we seek to find an antenna-independent capacity of a continuous-time system constrained only by the transmitters volume.

The system studied in this thesis is now described and a mathematical form is derived for it using electromagnetic theory. This will form the basis for further analysis in the next chapter.

We consider a transmitter that consists of a spherical volume which is a continuous array composed of an infinite number of antennas separated by infinitesimal distances as the transmitter as illustrated in Fig. 2.3. This eliminates the need to specify *a priori* the number of antennas and their relative positions on the antenna arrays. Each infinitesimal antenna is capable of generating an arbitrary 3-d current distribution.

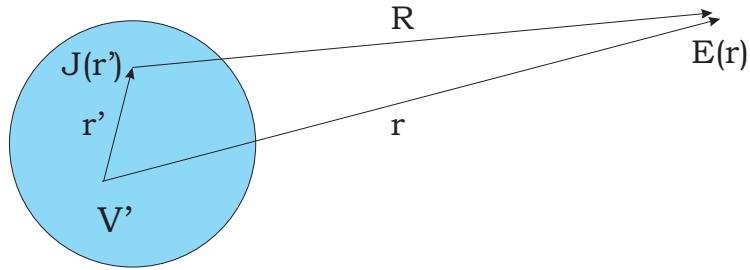


Figure 2.3: Signal Model

The spherical volume is constrained to have radius  $a$  making its effective aperture  $\mathcal{A}$  equal to  $\pi a^2$  and its volume  $V'$  equal to  $(4/3)\pi a^3$ . We assume that the radiated signals propagate in all directions, so that the channel solid angle  $|\Omega|$  corresponding to the angular spread is equal to  $4\pi$ . The current distribution generated by the antennas and the electric fields produced by it are time-varying sinusoidal electromagnetic quantities which can be represented as

$$\mathbf{J}(\mathbf{r}', t) = \text{Re}\{\mathbf{J}(\mathbf{r}')e^{ik_0ct}\} \quad \text{and} \quad \mathbf{E}(\mathbf{r}, t) = \text{Re}\{\mathbf{E}(\mathbf{r})e^{ik_0ct}\} \quad (2.14)$$

where  $\mathbf{J}(\mathbf{r}')$  and  $\mathbf{E}(\mathbf{r})$  are the complex-baseband representations for the current distribution at location  $\mathbf{r}'$  and electric field at location  $\mathbf{r}$  respectively,  $k_0 = 2\pi/\lambda$  with  $\lambda$  being the wavelength of the sinusoids and  $c$  is the speed of the electromagnetic waves. We will use the complex-baseband forms to represent the electromagnetic quantities hereafter.

Consider an antenna contained within a sphere of volume  $V'$ . We are interested in the electric field  $\mathbf{E}(\mathbf{r})$  at the receiver located at a point  $\mathbf{r}$  in space due to the

current distribution  $\mathbf{J}(\mathbf{r}')$  generated by the antenna elements within the spherical volume. We assume the receiver to be the entire surface of a sphere surrounding the transmitter and having a radius  $r$ . From Maxwell's equations, the electric field  $\mathbf{E}(\mathbf{r})$  due to current distribution  $\mathbf{J}(\mathbf{r}')$  is given by the following expression [8]

$$(-\nabla_{\mathbf{r}'} \times \nabla_{\mathbf{r}'} \times + k_0^2) \mathbf{E}(\mathbf{r}') = ik_0 \eta \mathbf{J}(\mathbf{r}') \quad (2.15)$$

where  $\eta$  is the intrinsic impedance. The solution to this equation can be written as an integral transform

$$\mathbf{E}(\mathbf{r}) = \int_{V'} \mathbf{G}(\mathbf{r}, \mathbf{r}') \mathbf{J}(\mathbf{r}') dV' \quad (2.16)$$

for some kernel  $\mathbf{G}(\mathbf{r}, \mathbf{r}')$ . The kernel  $\mathbf{G}(\mathbf{r}, \mathbf{r}')$  is often referred to as the Green's function in electromagnetic theory, where it is commonly derived for a particular coordinate system. A coordinate-free kernel has been derived in [8] and is given by

$$\mathbf{G}(\mathbf{r}, \mathbf{r}') = \frac{i\eta e^{ik_0 R}}{2\lambda R} \left[ \left( \mathbf{I} - \hat{\mathbf{R}}\hat{\mathbf{R}}^\dagger \right) + \frac{i}{k_0 R} \left( \mathbf{I} - 3\hat{\mathbf{R}}\hat{\mathbf{R}}^\dagger \right) - \frac{1}{k_0^2 R^2} \left( \mathbf{I} - 3\hat{\mathbf{R}}\hat{\mathbf{R}}^\dagger \right) \right] \quad (2.17)$$

where  $\mathbf{r} = r\hat{\mathbf{r}}$ ,  $\mathbf{r}' = r'\hat{\mathbf{r}}'$ ,  $\mathbf{R} = R\hat{\mathbf{R}}$  with  $\hat{\mathbf{r}}, \hat{\mathbf{r}}', \hat{\mathbf{R}}$  being the respective unit vectors and  $\mathbf{R}$  equals  $\mathbf{r} - \mathbf{r}'$ . The Green's function  $\mathbf{G}(\mathbf{r}, \mathbf{r}')$  gives the electric field at the observation point  $\mathbf{r}$  due to an impulsive current source at point  $\mathbf{r}'$ . It has three terms: far-field, intermediate-field and near-field. Since the electric field for the first term falls off inversely with the distance from the transmitter  $R$ , its power follows the inverse square law. The power of the remaining two terms falls off much faster than  $R^{-2}$  ( $R^{-4}$  and  $R^{-6}$ , respectively). Since in this thesis we are mainly interested in the electric field at a receiver located far from the transmitter, the contributions from the

near- and intermediate-field terms can be neglected. Neglecting the two terms, the expression for  $\mathbf{G}(\mathbf{r}, \mathbf{r}')$  becomes

$$\mathbf{G}(\mathbf{r}, \mathbf{r}') = \frac{i\eta e^{ik_0 R}}{2\lambda R} (\mathbf{I} - \hat{\mathbf{R}}\hat{\mathbf{R}}^\dagger) \quad (2.18)$$

For  $r \gg r'$  we have the following approximations

$$1/R \approx 1/r, \quad R \approx r - \hat{\mathbf{r}}^\dagger \mathbf{r}', \quad \text{and} \quad \hat{\mathbf{R}} \approx \hat{\mathbf{r}}$$

Making these substitutions in (2.18), we get

$$\mathbf{G}(\mathbf{r}, \mathbf{r}') = \frac{i\eta e^{ik_0 r}}{2\lambda r} (\mathbf{I} - \hat{\mathbf{r}}\hat{\mathbf{r}}^\dagger) e^{-ik_0 \hat{\mathbf{r}}^\dagger \mathbf{r}'} \quad (2.19)$$

and substituting for  $\mathbf{G}(\mathbf{r}, \mathbf{r}')$  in (2.16), we get

$$\mathbf{E}(\mathbf{r}) = \frac{i\eta e^{ik_0 r}}{2\lambda r} (\mathbf{I} - \hat{\mathbf{r}}\hat{\mathbf{r}}^\dagger) \int_{V'} e^{-ik_0 \hat{\mathbf{r}}^\dagger \mathbf{r}'} \mathbf{J}(\mathbf{r}') dV' \quad (2.20)$$

The above expression gives the continuous-time relation between the radiated electric field  $\mathbf{E}(\mathbf{r})$  (the system output) and the current distribution  $\mathbf{J}(\mathbf{r}')$  (the system input) generated by the antennas inside the sphere of volume  $V'$ . In the next chapter, we will analyze this system in greater detail.

## Chapter 3

# A Discrete-Time Equivalent System and its Analysis

In order to find the capacity of a system in an antenna-independent way, we introduced a continuous-time model in the previous chapter. We also derived a continuous-time relation (2.20) between the system input (current distributions at the transmitter) and the system output (electric field at the receiver) for that system. However, the continuous-time formulation of the system makes it difficult to perform the capacity analysis and carry out numerical simulations. Therefore, to make the analysis more tractable, we will reduce the continuous-time system to an equivalent discrete-time form in this chapter. Orthonormal basis expansions will be used to reduce the continuous-time electromagnetic quantities to their discrete-time

counterparts. The discrete-time system can then be represented in matrix form which becomes equivalent to a MIMO system, thereby enabling us to use the capacity expressions for MIMO systems reviewed in the previous chapter.

In the next two sections we perform the discrete-time system reduction for two different scenarios. First, we look at a system in which the transmitter antennas have 3-d current distributions, i.e. the antennas excite all the three polarizations and therefore the vector  $\mathbf{J}(\mathbf{r}')$  consists of three components  $J_x(\mathbf{r}')$ ,  $J_y(\mathbf{r}')$  and  $J_z(\mathbf{r}')$ . The receiver antennas in this case are such that they can capture information from all three components  $E_x(\mathbf{r})$ ,  $E_y(\mathbf{r})$  and  $E_z(\mathbf{r})$  of the received electric field. It is important to note here that since the magnetic field is given by the curl of the electric field [8] for this system, we would not extract any more information by observing the magnetic field also.

Since most of the existing antenna systems consist of dipoles which can only generate 1-d current distributions, we will also look at such a system in the second case. For this system, the transmitter antennas can only generate 1-d current distributions, however, the receiver is still capable of capturing the entire radiated electromagnetic field in the far-field of the transmitter.

## 3.1 An Orthonormal Basis for the Electric Field

### 3.1.1 3-d Current Distributions

Expanding the vectors  $\mathbf{E}(\mathbf{r})$  and  $\mathbf{J}(\mathbf{r}')$  in terms of their components  $E_x(\mathbf{r})$ ,  $E_y(\mathbf{r})$ ,  $E_z(\mathbf{r})$  and  $J_x(\mathbf{r}')$ ,  $J_y(\mathbf{r}')$ ,  $J_z(\mathbf{r}')$ , respectively, and writing (2.20) in matrix form, we get

$$\begin{bmatrix} E_x(\mathbf{r}) \\ E_y(\mathbf{r}) \\ E_z(\mathbf{r}) \end{bmatrix} = (\mathbf{I} - \hat{\mathbf{r}}\hat{\mathbf{r}}^\dagger) \begin{bmatrix} k_1 \int_{V'} e^{-ik_0\hat{\mathbf{r}}^\dagger\mathbf{r}'} J_x(\mathbf{r}') dV' \\ k_1 \int_{V'} e^{-ik_0\hat{\mathbf{r}}^\dagger\mathbf{r}'} J_y(\mathbf{r}') dV' \\ k_1 \int_{V'} e^{-ik_0\hat{\mathbf{r}}^\dagger\mathbf{r}'} J_z(\mathbf{r}') dV' \end{bmatrix} \quad (3.1)$$

where  $k_1 = \frac{i\eta e^{ik_0 r}}{2\lambda r}$  is a constant. Let us define

$$F_x(\mathbf{r}) = k_1 \int_{V'} e^{-ik_0\hat{\mathbf{r}}^\dagger\mathbf{r}'} J_x(\mathbf{r}') dV' \quad (3.2)$$

with  $F_y(\mathbf{r})$  and  $F_z(\mathbf{r})$  defined similarly.

To evaluate the expression for  $F_x(\mathbf{r})$ , we will write the terms  $e^{-ik_0\hat{\mathbf{r}}^\dagger\mathbf{r}'}$  and  $J_x(\mathbf{r}')$  in terms of their series expansions. To this end, it is helpful to express the problem in spherical coordinates,  $\mathbf{r} = (r, \theta, \varphi)$  and  $\mathbf{r}' = (r', \theta', \varphi')$  with  $\varphi$  being the azimuth and  $\theta$  the elevation. Also  $\hat{\mathbf{r}}^\dagger\mathbf{r}'$  equals  $r' \cos \vartheta$  where  $\vartheta$  is the angle between  $\mathbf{r}$  and  $\mathbf{r}'$ , which is given implicitly by  $\cos \vartheta = \sin \theta \sin \theta' \cos(\varphi - \varphi') + \cos \theta \cos \theta'$ .

The term  $e^{-ik_0\hat{\mathbf{r}}^\dagger\mathbf{r}'}$  can be written in terms of the spherical Bessel functions [20,

pp. 428]. Its series expansion is given by

$$e^{-ik_0\hat{\mathbf{r}}^\dagger\mathbf{r}'} = 4\pi \sum_{n=0}^{\infty} \sum_{m=-n}^n (-i)^n j_n(k_0r') Y_{n,m}(\theta, \varphi) Y_{n,m}^*(\theta', \varphi') \quad (3.3)$$

where  $j_n$  is the spherical Bessel function of first kind of order  $n$  and  $\{Y_{n,m}\}$ , which is the set of spherical harmonics, forms a complete orthonormal basis over the surface of a unit sphere. The  $*$  operator in the expression denotes complex conjugation. The spherical harmonics  $\{Y_{n,m}\}$  are defined as [19, pp. 244]

$$Y_{n,m}(\theta, \varphi) = \sqrt{\frac{(2n+1)(n-m)!}{4\pi(n+m)!}} P_n^m(\cos\theta) e^{im\varphi}, \quad m = 0, \pm 1, \pm 2, \dots, \pm n \quad (3.4)$$

and satisfy the following orthonormal relations

$$\int_0^\pi \int_0^{2\pi} Y_{n,m}^*(\theta, \varphi) Y_{n',m'}(\theta, \varphi) \sin\theta d\varphi d\theta = \delta_{m,m'} \delta_{n,n'} \quad (3.5)$$

where  $P_n^m(\cdot)$  is the associated Legendre function. For ease of notation, we will represent the double summation  $\sum_{n=0}^{\infty} \sum_{m=-n}^n$  by  $\sum_{|m|\leq n}$  and  $Y_{n,m}(\theta, \varphi)$  by  $Y_{n,m}$  in the rest of this thesis.

Now, let  $\mathcal{X}$  be the space spanned by the set  $\{j_{n'}(k_0r') Y_{n',m'}(\theta', \varphi')\}$  for  $n' \in \{0 \dots \infty\}$  and  $m' \in \{-n', \dots, n'\}$ . Then  $\mathcal{X}$  forms a subspace of  $\mathcal{L}^2$ , where

$$\mathcal{L}^2 \equiv L^2([0, a] \times [0, \pi] \times [0, 2\pi]) \quad (3.6)$$

$\mathcal{L}^2$  is the space of all square-integrable functions over the domain  $([0, a] \times [0, \pi] \times [0, 2\pi])$  which represents a sphere of radius  $a$ . If  $J_x(\mathbf{r}')$  is square-integrable over the domain, then it lies in  $\mathcal{L}^2$  and can be written as a sum of two components,  $J_x \in \mathcal{X}$  and

$J_x^\perp \in \mathcal{X}^\perp$ , where  $\mathcal{X}^\perp$  is the orthogonal space to  $\mathcal{X}$ . Since  $J_x^\perp$  lies in the orthogonal space of the operator at hand, it will not contribute to the system output and can be neglected. Thus, we can write  $J_x(\mathbf{r}')$  as

$$J_x(\mathbf{r}') = \sum_{|m'| \leq n'} c_{n',m'}^x j_{n'}(k_0 r') Y_{n',m'}(\theta', \varphi') \quad (3.7)$$

Now, substituting the series expansion of  $e^{-ik_0 \hat{\mathbf{r}}^\dagger \mathbf{r}'}$  and  $J_x(\mathbf{r}')$  from (3.3) and (3.7), respectively, into the expression for  $F_x(\mathbf{r})$  in (3.2), we get

$$\begin{aligned} F_x(\mathbf{r}) &= 4\pi k_1 \int_{V'} \sum_{|m| \leq n} (-i)^n j_n(k_0 r') Y_{n,m}(\theta, \varphi) Y_{n,m}^*(\theta', \varphi') \\ &\quad \sum_{|m'| \leq n'} c_{n',m'}^x j_{n'}(k_0 r') Y_{n',m'}(\theta', \varphi') dV' \\ &= 4\pi k_1 \int_0^{2\pi} \int_0^\pi \int_0^a \sum_{|m| \leq n} (-i)^n j_n(k_0 r') Y_{n,m}(\theta, \varphi) Y_{n,m}^*(\theta', \varphi') \\ &\quad \sum_{|m'| \leq n'} c_{n',m'}^x j_{n'}(k_0 r') Y_{n',m'}(\theta', \varphi') r'^2 \sin(\theta') dr' d\theta' d\varphi' \end{aligned} \quad (3.8)$$

Using (3.5), the above expression reduces to

$$\begin{aligned} F_x(\mathbf{r}) &= 4\pi k_1 \int_0^a \sum_{|m| \leq n} (-i)^n j_n(k_0 r') Y_{n,m}(\theta, \varphi) \sum_{|m'| \leq n'} c_{n',m'}^x j_{n'}(k_0 r') \delta_{nn'} \delta_{mm'} r'^2 dr' \\ &= 4\pi k_1 \sum_{|m| \leq n} c_{n,m}^x Y_{n,m}(\theta, \varphi) (-i)^n \int_0^a j_n^2(k_0 r') r'^2 dr' \\ &= \sum_{|m| \leq n} \beta_{n,m}^x Y_{n,m}(\theta, \varphi) \end{aligned} \quad (3.9)$$

where  $\beta_{n,m}^x = c_{n,m}^x \alpha_n$  and

$$\alpha_n = 4\pi k_1 (-i)^n \frac{1}{k_0^3} \int_0^{k_0 a} j_n^2(r'') r''^2 dr'' \quad (3.10)$$

with  $r'' = k_0 r'$ . Following the same procedure, the expressions for  $F_y(\mathbf{r})$  and  $F_z(\mathbf{r})$

are

$$F_y(\mathbf{r}) = \sum_{|m| \leq n} \beta_{n,m}^y Y_{n,m}(\theta, \varphi) \quad , \quad F_z(\mathbf{r}) = \sum_{|m| \leq n} \beta_{n,m}^z Y_{n,m}(\theta, \varphi) \quad (3.11)$$

The relation between  $\beta_{n,m}^x$ ,  $c_{n,m}^x$  and  $\alpha_n$  can be written in matrix form as follows.

$$\underbrace{\begin{bmatrix} \beta_{0,0}^x \\ \beta_{1,-1}^x \\ \beta_{1,0}^x \\ \beta_{1,1}^x \\ \vdots \\ \vdots \\ \beta_{n_{max}-1, n_{max}-1}^x \end{bmatrix}}_{B_x} = \underbrace{\begin{bmatrix} \alpha_0 & \cdots & \cdots & 0 \\ & \alpha_1 & & \\ & & \alpha_1 & \vdots \\ \vdots & & & \alpha_1 & \vdots \\ \vdots & & & & \ddots \\ \vdots & & & & & \ddots \\ 0 & \cdots & & & & \alpha_{n_{max}} \end{bmatrix}}_A \underbrace{\begin{bmatrix} c_{0,0}^x \\ c_{1,-1}^x \\ c_{1,0}^x \\ c_{1,1}^x \\ \vdots \\ \vdots \\ c_{n_{max}-1, n_{max}-1}^x \end{bmatrix}}_{C_x} \quad (3.12)$$

In the expression above, the index  $n$  which varies from 0 to  $\infty$  has been restricted to a finite number  $n_{max}$ . This truncation may result in some error. Using numerical simulations in Section 4.1 and an analysis in Appendix B, we show that by choosing  $n_{max}$  sufficiently large, the error caused due to truncation becomes very small and goes to zero as  $n_{max}$  goes to  $\infty$ . By restricting  $n$  to  $n_{max}$ ,  $B_x$  and  $C_x$  reduce to  $n_{max}^2 \times 1$  matrices and  $A$  reduces to an  $n_{max}^2 \times n_{max}^2$  matrix. Similarly, we have  $B_y = AC_y$  and  $B_z = AC_z$  corresponding to the  $y, z$  components as well. Combining the matrix

equations for the three components  $B_x, B_y$  and  $B_z$  we get

$$\begin{bmatrix} B_x \\ B_y \\ B_z \end{bmatrix} = \begin{bmatrix} A & \mathbf{0} & \mathbf{0} \\ \mathbf{0} & A & \mathbf{0} \\ \mathbf{0} & \mathbf{0} & A \end{bmatrix} \begin{bmatrix} C_x \\ C_y \\ C_z \end{bmatrix} \quad (3.13)$$

where  $\mathbf{0}$  denotes an  $n_{max}^2 \times n_{max}^2$  matrix of zeros.

Let us next give the expansion for the  $3 \times 3$  matrix  $(\mathbf{I} - \hat{\mathbf{r}}\hat{\mathbf{r}}^\dagger)$ . Since

$$\hat{\mathbf{r}} = (\sin \theta \cos \varphi, \sin \theta \sin \varphi, \cos \theta)^T$$

$(\mathbf{I} - \hat{\mathbf{r}}\hat{\mathbf{r}}^\dagger)$  can be written as

$$(\mathbf{I} - \hat{\mathbf{r}}\hat{\mathbf{r}}^\dagger) = \begin{bmatrix} 1 - \sin^2(\theta) \cos^2(\varphi) & \sin^2(\theta) \sin(\varphi) \cos(\varphi) & \sin(\theta) \cos(\theta) \cos(\varphi) \\ \sin^2(\theta) \sin(\varphi) \cos(\varphi) & 1 - \sin^2(\theta) \sin^2(\varphi) & \sin(\theta) \cos(\theta) \sin(\varphi) \\ \sin(\theta) \cos(\theta) \cos(\varphi) & \sin(\theta) \cos(\theta) \sin(\varphi) & 1 - \cos^2(\theta) \end{bmatrix} \quad (3.14)$$

By substituting the expressions for  $F_x(\mathbf{r}), F_y(\mathbf{r}), F_z(\mathbf{r})$  from (3.9), (3.11) and the expansion for  $(\mathbf{I} - \hat{\mathbf{r}}\hat{\mathbf{r}}^\dagger)$  from (3.14) into the matrix equation (3.1), we get

$$\begin{bmatrix} E_x(\mathbf{r}) \\ E_y(\mathbf{r}) \\ E_z(\mathbf{r}) \end{bmatrix} = \begin{bmatrix} r_{11} & r_{12} & r_{13} \\ r_{21} & r_{22} & r_{23} \\ r_{31} & r_{32} & r_{33} \end{bmatrix} \begin{bmatrix} \sum_{|m| \leq n} \beta_{n,m}^x Y_{n,m} \\ \sum_{|m| \leq n} \beta_{n,m}^y Y_{n,m} \\ \sum_{|m| \leq n} \beta_{n,m}^z Y_{n,m} \end{bmatrix} \quad (3.15)$$

where the first matrix on the right-hand side with  $(r_{11}, r_{12}, \dots)$  has been used to represent the  $(\mathbf{I} - \hat{\mathbf{r}}\hat{\mathbf{r}}^\dagger)$  matrix for ease of notation.

From the expression above, the electric field component  $E_x(\mathbf{r})$  can be written as

$$E_x(\mathbf{r}) = \sum_{|m| \leq n} \beta_{n,m}^x r_{11} Y_{n,m} + \sum_{|m| \leq n} \beta_{n,m}^y r_{12} Y_{n,m} + \sum_{|m| \leq n} \beta_{n,m}^z r_{13} Y_{n,m} \quad (3.16)$$

We now state two facts regarding the spherical harmonics  $Y_{n,m}$  :

1. The mappings  $\cos \theta Y_{n,m}$  ,  $\sin \theta e^{\pm i\varphi} Y_{n,m}$  reduce to linear transformations from the space formed by  $\text{span}\{Y_{n,m}\}$  to itself because of recurrence relations.
2. All the terms of  $(\mathbf{I} - \hat{\mathbf{r}}\hat{\mathbf{r}}^\dagger)Y_{n,m}$  can therefore be written as successive transformations mentioned above.

Using these facts, we can write  $r_{11}Y_{n,m}$ ,  $r_{12}Y_{n,m}$  and  $r_{13}Y_{n,m}$  as

$$\begin{aligned} r_{11}Y_{n,m} &= \sum_{|m'| \leq n'} \gamma_{11,(n'm')}^{n,m} Y_{n',m'} \\ r_{12}Y_{n,m} &= \sum_{|m'| \leq n'} \gamma_{12,(n'm')}^{n,m} Y_{n',m'} \\ r_{13}Y_{n,m} &= \sum_{|m'| \leq n'} \gamma_{13,(n'm')}^{n,m} Y_{n',m'} \end{aligned}$$

where  $\gamma$  represent the new coefficients. In Appendix A, we give the recurrence relations and also a procedure for calculating the coefficient values using these recurrence

relations. Here we use  $\gamma$  only for notation. Therefore (3.16) becomes

$$\begin{aligned}
E_x(\mathbf{r}) &= \sum_{|m| \leq n} \beta_{n,m}^x \sum_{|m'| \leq n'} \gamma_{11,(n'm')}^{n,m} Y_{n',m'} + \sum_{|m| \leq n} \beta_{n,m}^y \sum_{|m'| \leq n'} \gamma_{12,(n'm')}^{n,m} Y_{n',m'} + \\
&\quad \sum_{|m| \leq n} \beta_{n,m}^z \sum_{|m'| \leq n'} \gamma_{13,(n'm')}^{n,m} Y_{n',m'} \\
&= \sum_{|m'| \leq n'} \sum_{|m| \leq n} \beta_{n,m}^x \gamma_{11,(n'm')}^{n,m} Y_{n',m'} + \sum_{|m'| \leq n'} \sum_{|m| \leq n} \beta_{n,m}^y \gamma_{12,(n'm')}^{n,m} Y_{n',m'} + \\
&\quad \sum_{|m'| \leq n'} \sum_{|m| \leq n} \beta_{n,m}^z \gamma_{13,(n'm')}^{n,m} Y_{n',m'} \\
&= \sum_{|m'| \leq n'} \underbrace{\left[ \sum_{|m| \leq n} \beta_{n,m}^x \gamma_{11,(n'm')}^{n,m} + \sum_{|m| \leq n} \beta_{n,m}^y \gamma_{12,(n'm')}^{n,m} + \sum_{|m| \leq n} \beta_{n,m}^z \gamma_{13,(n'm')}^{n,m} \right]}_{d_{n',m'}^x} Y_{n',m'}
\end{aligned} \tag{3.17}$$

The electric field components  $E_y$  and  $E_z$  can be derived similarly and are given by

$$E_y(\mathbf{r}) = \sum_{|m'| \leq n'} d_{n',m'}^y Y_{n',m'} \quad , \quad E_z(\mathbf{r}) = \sum_{|m'| \leq n'} d_{n',m'}^z Y_{n',m'} \tag{3.18}$$

where the  $d_{n',m'}$  represent the coefficients in the discrete expansion of the electric field components in terms of the basis functions  $Y_{n',m'}$ .

The relationship between the  $d$ ,  $\gamma$  and  $\beta$  coefficients can be written using (3.17)

in matrix form as

$$\begin{bmatrix} D_x \\ D_y \\ D_z \end{bmatrix} = \begin{bmatrix} \Gamma_{11} & \Gamma_{12} & \Gamma_{13} \\ \Gamma_{21} & \Gamma_{22} & \Gamma_{23} \\ \Gamma_{31} & \Gamma_{32} & \Gamma_{33} \end{bmatrix} \begin{bmatrix} B_x \\ B_y \\ B_z \end{bmatrix} \tag{3.19}$$

where  $D_x$  represents the coefficients  $d_{n',m'}^x$  for  $|m'| \leq n'$  and  $n' \in \{0 \dots \infty\}$ . Similarly  $D_y$  and  $D_z$  represent the  $d_{n',m'}^y$  and  $d_{n',m'}^z$  coefficients respectively. Also,  $\Gamma$  can be

further expanded. For example, by varying  $(n', m')$  along the rows and  $(n, m)$  along the columns,  $\Gamma_{11}$  can be written as,

$$\Gamma_{11} = \begin{bmatrix} \gamma_{11(0,0)}^{(0,0)} & \gamma_{11(0,0)}^{(1,-1)} & \gamma_{11(0,0)}^{(1,0)} & \gamma_{11(0,0)}^{(1,1)} & \cdots & \gamma_{11(0,0)}^{(n_{max}-1, n_{max}-1)} \\ \gamma_{11(1,-1)}^{(0,0)} & \ddots & & & & \\ \gamma_{11(1,0)}^{(0,0)} & & \ddots & & & \\ \gamma_{11(1,1)}^{(0,0)} & & & & & \vdots \\ \vdots & & & & \ddots & \\ \gamma_{11(n_{max}-1, n_{max}-1)}^{(0,0)} & & & & & \gamma_{11(n_{max}-1, n_{max}-1)}^{(n_{max}-1, n_{max}-1)} \end{bmatrix} \quad (3.20)$$

Expanding expression (3.19) by substituting for vector  $(B_x, B_y, B_z)^T$  using (3.13), gives us the important system input-output equation in discrete form

$$\begin{bmatrix} D_x \\ D_y \\ D_z \end{bmatrix} = \underbrace{\begin{bmatrix} \Gamma_{11} & \Gamma_{12} & \Gamma_{13} \\ \Gamma_{21} & \Gamma_{22} & \Gamma_{23} \\ \Gamma_{31} & \Gamma_{32} & \Gamma_{33} \end{bmatrix}}_{\mathbf{\Gamma}} \underbrace{\begin{bmatrix} A & \mathbf{0} & \mathbf{0} \\ \mathbf{0} & A & \mathbf{0} \\ \mathbf{0} & \mathbf{0} & A \end{bmatrix}}_{\mathbf{A}} \begin{bmatrix} C_x \\ C_y \\ C_z \end{bmatrix} \quad (3.21)$$

where the left-hand side coefficient vector  $(D_x, D_y, D_z)^T$  represents the radiated electric field  $\mathbf{E}(\mathbf{r})$  due to current distributions  $\mathbf{J}(\mathbf{r}')$ , which is represented by the right-hand side coefficient vector  $(C_x, C_y, C_z)^T$  in the above expression.

### 3.1.2 1-d Current Distributions

We now consider the case of 1-d current distributions in which the current density vector has only one non-zero component, say  $J_x(\mathbf{r}')$ . Then the matrix equivalent of equation (2.20) for this case is

$$\begin{bmatrix} E_x(\mathbf{r}) \\ E_y(\mathbf{r}) \\ E_z(\mathbf{r}) \end{bmatrix} = (\mathbf{I} - \hat{\mathbf{r}}\hat{\mathbf{r}}^\dagger) \begin{bmatrix} k_1 \int_{V'} e^{-ik_0\hat{\mathbf{r}}^\dagger\mathbf{r}'} J_x(\mathbf{r}') dV' \\ 0 \\ 0 \end{bmatrix} \quad (3.22)$$

The analysis for 1-d current distributions is a particular case of the analysis for 3-d current distributions. Since the components  $C_y$  and  $C_z$  are zero for the 1-d case, the vector of coefficients representing the series expansion of the current density vector becomes  $(C_x, 0, 0)^T$ . Also since  $C_y$  and  $C_z$  are zero, the components  $B_y$  and  $B_z$  in (3.13) also become zero. The coefficients in the series expansion of the electric field for the 1-d case can therefore be written as

$$\begin{bmatrix} D_x^{1d} \\ D_y^{1d} \\ D_z^{1d} \end{bmatrix} = \begin{bmatrix} \Gamma_{11} \\ \Gamma_{21} \\ \Gamma_{31} \end{bmatrix} \begin{bmatrix} B_x \end{bmatrix} \quad (3.23)$$

and the discrete-system input-output equation for the 1-d case becomes

$$\begin{bmatrix} D_x^{1d} \\ D_y^{1d} \\ D_z^{1d} \end{bmatrix} = \begin{bmatrix} \Gamma_{11} \\ \Gamma_{21} \\ \Gamma_{31} \end{bmatrix} \begin{bmatrix} A \end{bmatrix} \begin{bmatrix} C_x \end{bmatrix} \quad (3.24)$$

where again the left-hand side coefficient vector  $(D_x^{1d}, D_y^{1d}, D_z^{1d})^T$  represents the radiated electric field  $\mathbf{E}(\mathbf{r})$  due to the current distribution  $\mathbf{J}(\mathbf{r}')$ , which is represented by the right hand-side coefficient vector  $(C_x)^T$  in the above expression.

## 3.2 Normalization and Capacity Calculations

Before we move on to the capacity calculations for our system, we need to determine the power normalization to be applied to the capacity formulas derived in the previous chapter to get meaningful results. The normalization is an important aspect, both for analyzing the absolute capacity results as well as in comparing capacities for different systems. The normalization is carried out with respect to the signal-to-noise ratio (or SNR) at the receiver for the MIMO system. Therefore, we first derive the SNR for the MIMO system and then work out the normalization.

### 3.2.1 Signal-to-Noise Ratio

To calculate the SNR at the receiver for the MIMO system we first rewrite the MIMO system equation (2.1)

$$\mathbf{y} = \sqrt{\frac{P}{N_t}} \mathbf{H} \mathbf{x} + \mathbf{n} \quad (3.25)$$

We assume the elements of  $\mathbf{H}$ ,  $h_{ij}$  ( $i = 1, \dots, N_r$ ,  $j = 1, \dots, N_t$ ) are normalized so that  $\mathcal{E}\{|h_{ij}|^2\} = 1$ . We also assume equal power distribution at the transmitter antennas

i.e.  $\mathbf{Q} = \mathbf{I}_{N_t}$ . For a particular channel realization  $\mathbf{H} = H$ , we can write

$$\begin{aligned}\mathcal{E}\{|\mathbf{y}|^2\} &= \frac{P}{N_t} \text{Tr}\{H \mathcal{E}(\mathbf{x}\mathbf{x}^\dagger) H^\dagger\} + \text{Tr}\{\mathcal{E}(\mathbf{n}\mathbf{n}^\dagger)\} \\ &= \frac{P}{N_t} \text{Tr}\{H H^\dagger\} + N_r\end{aligned}\tag{3.26}$$

Averaging over various channel realizations, we get

$$\begin{aligned}\mathcal{E}\{|\mathbf{y}|^2\} &= \frac{P}{N_t} \text{Tr}\{\mathcal{E}(\mathbf{H}\mathbf{H}^\dagger)\} + N_r \\ &= \frac{P N_t N_r}{N_t} + N_r\end{aligned}\tag{3.27}$$

From the expression above we get the average SNR at the receiver to be  $P$ .

### 3.2.2 Normalization

Let us now look at a modified MIMO system model defined as

$$\mathbf{y} = k \sqrt{\frac{P}{N_t}} \mathbf{H}\mathbf{x} + \mathbf{n}\tag{3.28}$$

where  $k$  is a constant and the entries  $h_{ij}$  of  $\mathbf{H}$  in general do not satisfy  $\mathcal{E}\{|h_{ij}|^2\} = 1$ .

In this case, we would like to normalize the system by choosing the constant  $k$  in a way such that the received SNR of the system remains the same as the previous system,

i.e. equal to  $P$ . Again assuming equal power distribution at the transmitter antennas

i.e.  $\mathbf{Q} = \mathbf{I}_{N_t}$  and following the same procedure as we did in the previous section, the

received SNR for this modified system can be shown to be equal to  $\frac{k^2 P}{N_t N_r} \text{Tr}\{\mathcal{E}(\mathbf{H}\mathbf{H}^\dagger)\}$ .

Now, we want to calculate the normalization constant  $k$  such that the SNR is the

same as in the previous case, i.e. we need to solve

$$\frac{k^2 P}{N_t N_r} \text{Tr}\{\mathcal{E}(\mathbf{H}\mathbf{H}^\dagger)\} = P \quad (3.29)$$

The above expression gives us the value of  $k$  as

$$k = \frac{\sqrt{N_t N_r}}{\sqrt{\text{Tr}\{\mathcal{E}(\mathbf{H}\mathbf{H}^\dagger)\}}} \quad (3.30)$$

### 3.2.3 Capacity Calculations for Our System

Let us now use the previous results on channel capacity and normalization to analyze the capacities for our system. For the case of 3-d current distributions, recall from equation (3.21), that  $\mathbf{\Gamma}\mathbf{A}$  connects the system input to the system output and therefore can be thought of as being equivalent to the channel matrix  $\mathbf{H}$  for the MIMO system. However, it should be noted here that the  $\mathbf{\Gamma}\mathbf{A}$  matrix is a deterministic quantity unlike  $\mathbf{H}$  (which was random) for the MIMO systems considered in the previous chapter and therefore the expectation operator  $\mathcal{E}$  will fall out of the capacity and normalization constant formulas. For our capacity calculations, we proceed as follows. First, we define a baseline system. We use this system to calculate the normalization constant  $k$  such that the received SNR is equal to  $P$ . The spherical volume at the transmitter is assumed to have a radius of  $1\lambda$  for the baseline system. We also assume equal power distribution i.e.  $\mathbf{Q} = \mathbf{I}_{N_t}$  at the transmitter for this system. Let  $\mathbf{\Gamma}_b, \mathbf{A}_b$  denote the  $\mathbf{\Gamma}, \mathbf{A}$  matrices for this system. Then, from equation

(3.30) and the fact that  $\mathbf{H} = \mathbf{\Gamma}_b \mathbf{A}_b$ , we get

$$k = \frac{\sqrt{N_t N_r}}{\sqrt{\text{Tr}\{\mathbf{\Gamma}_b \mathbf{A}_b \mathbf{A}_b^\dagger \mathbf{\Gamma}_b^\dagger\}}} \quad (3.31)$$

Once we know  $k$ , we can now calculate the capacity for the baseline system from (2.6)

as

$$C = \sum_{i=1}^r \log_2 \left( 1 + k^2 \frac{P}{N_t} \lambda_i \right) \quad (3.32)$$

where  $k$  is defined in (3.31),  $r$  is the rank of the hermitian matrix  $\mathbf{\Gamma}_b \mathbf{A}_b \mathbf{A}_b^\dagger \mathbf{\Gamma}_b^\dagger$  and  $(\lambda_1, \dots, \lambda_r)$  are its positive eigenvalues in decreasing order. It should be noted here that since we assumed an equal-power distribution at the transmitter, the capacity calculated here corresponds to the NCSI case. The capacity values corresponding to the CSI case for this system would be larger. However, the purpose of this system is only to find the normalization constant and to get a baseline capacity, which would enable us to calculate capacities for other systems and to make meaningful comparisons.

Having calculated the normalization constant and capacity for the baseline system, we now consider other systems and compare how they perform with respect to this baseline system. First, we calculate the capacity for a system having the same size as the baseline system ( $a = 1\lambda$ ), but now we use CSI case for capacity calculations, i.e. power allocation is done using the optimal water-pouring scheme. The same normalization constant is used that was calculated for the baseline system. This gives us the true capacity of the system with radius  $1\lambda$ . Next, we look at the capacities of

systems of different sizes and see how they compare with the capacity of the system having a radius of  $1\lambda$ . To this end, we vary the radius  $a$  of the transmitter shell between  $.5\lambda$  and  $4\lambda$  and calculate the capacities using the optimal power distribution. As we increase the size of the transmitter shell, we get more spatial degrees of freedom and the received SNR also increases. Similarly a decrease in size would correspond to fewer spatial degrees of freedom and received SNR. Since we want to correctly capture the change in capacity due to the change in transmitter size, we use the same normalization constant  $k$  as calculated for the baseline system. If instead we had calculated a new normalization constant for each transmitter size, we would not have captured the change in capacity due to a change in received SNR. Using the water-pouring algorithm for power allocation, the capacity for the system can be written using equation (2.13) as

$$C = \sum_{i=1}^{n^*} \log_2 \left( \mu \frac{k^2 P}{N_t} \lambda_i \right) \quad (3.33)$$

where  $n^* = \max\{i : (k^2 P \lambda_i / N_t)^{-1} \leq \mu\}$  is the number of eigenmodes getting positive power allocation and  $\mu$  is the constant satisfying

$$\sum_{i=1}^{n^*} \left( \mu - \frac{N_t}{k^2 P \lambda_i} \right) = N_t \quad (3.34)$$

Next, we calculate the capacities for the system with 1-d current distributions and different sizes. Again, in order to make meaningful comparisons with the capacities calculated for the 3-d counterparts, we use the same normalization constant  $k$  calculated earlier. The procedure for calculating the capacity for 1-d systems remains the same.

To proceed with the capacity calculations, we need to determine the  $\mathbf{\Gamma}$  and  $\mathbf{A}$  matrices, which can be done using results from Section 3.1.1. Once we have these matrices, we can proceed with the calculations.

### 3.3 Spatial Degrees of Freedom

Let us rewrite the input-output equation (3.21) for the system with 3-d current distributions

$$\begin{bmatrix} D_x \\ D_y \\ D_z \end{bmatrix} = \underbrace{\begin{bmatrix} \Gamma_{11} & \Gamma_{12} & \Gamma_{13} \\ \Gamma_{21} & \Gamma_{22} & \Gamma_{23} \\ \Gamma_{31} & \Gamma_{32} & \Gamma_{33} \end{bmatrix}}_{\mathbf{\Gamma}} \underbrace{\begin{bmatrix} A & 0 & 0 \\ 0 & A & 0 \\ 0 & 0 & A \end{bmatrix}}_{\mathbf{A}} \begin{bmatrix} C_x \\ C_y \\ C_z \end{bmatrix} \quad (3.35)$$

This is the discrete equivalent of the continuous-time input-output system, with the current distributions  $\mathbf{J}(\mathbf{r}')$  being the input and the radiated electric field  $\mathbf{E}(\mathbf{r})$  being the output. Since we are representing the continuous quantities  $\mathbf{J}(\mathbf{r}')$  and  $\mathbf{E}(\mathbf{r})$  in terms of the basis functions, the coefficient vectors  $(D_x, D_y, D_z)^T$ ,  $(C_x, C_y, C_z)^T$ , and therefore the matrix equation above is infinite-dimensional. Since the input-output system is infinite-dimensional, we therefore have infinitely many eigenmodes or spatial channels over which power can be transmitted. However, for a given size of the input spherical volume, only a finite number of these eigenmodes correspond to significant eigenvalues [9], with the number increasing with size of the input sphere. Therefore, given a power constraint at the transmitter, and the fact that there are only a finite

number of significant eigenvalues, we cannot allocate power to all of the eigenmodes. If we use the water-pouring algorithm for power allocation at the transmitter, only  $n^*$  of the eigenmodes would receive power. We define the number of eigenmodes receiving power  $n^*$  as the number of *spatial degrees of freedom* for our system.

In [8], Poon *et al.* derive an upper bound on the spatial degrees of freedom for linear arrays. They also give an upper bound for the spatial degrees of freedom for spherical arrays, but use heuristic arguments based on the resolvability of spherical arrays to derive the bound for spherical arrays. They claim that the spatial degrees of freedom for spherical arrays are upper bounded by  $\mathcal{A}|\Omega|$ , where  $\mathcal{A} = \pi a^2$  is the effective aperture of the spherical array with  $a$  being the radius and  $|\Omega|$  is a measure of the angular spread due to scattering, with the maximum value being  $4\pi$  in a fully scattered environment. Therefore the upper bound on the number of spatial degrees of freedom becomes  $4\pi^2 a^2$ , irrespective of the system SNR. Since this bound is derived using heuristic arguments, we would like to compare this with the results we get numerically using our system model. We show in the next chapter on simulation results that, although the results closely follow the claim that the spatial degrees of freedom is linearly dependent on the effective aperture, the scaling factor could be more than one, making the number of spatial degrees of freedom more than the claimed upper bound of  $4\pi^2 a^2$ . We also see an increase in the spatial degrees of freedom as we increase SNR. This is intuitive also, since, as we increase the available power at the transmitter, more of the infinitely many possible spatial channels would

now get power and hence the number of spatial degrees of freedom will also increase.

Another important aspect treated in [8] is the increase in spatial degrees of freedom by using 3-d current distributions (or tri-polarized antennas, as the authors call them) at the transmitter instead of 1-d current distributions (or uni-polarized antennas). The authors claim that the maximum increase in spatial degrees of freedom that we could achieve by using 3-d current distributions is a factor of two. Here, our simulation results tend to suggest that the spatial degrees of freedom can go up by 3 times using 3-d current distributions for sufficiently large spherical volumes. The increase in spatial degrees of freedom is between 2 and 3 times for input shells on the order of a few wavelengths.

As mentioned above, the true input-output system is infinite-dimensional, making it difficult to evaluate numerically. To overcome this problem and to be able to perform numerical calculations on the system, we reduce it to a finite-dimensional one. Earlier, in Section 2.2 also, we had briefly mentioned this reduction to a finite-dimensional system (equation 3.12). The system was reduced by truncating the number of  $\alpha, \beta$  and  $c$  coefficients from infinity to  $n_{max}$ . Since this truncation leads to a difference in the eigenvalues of the truncated system from those of the true system, we would like to quantize this error and also its effect on capacity calculations. An analysis is presented in Appendix B which shows that the truncation error goes to zero as the dimension of the truncated system goes to infinity. A set of upper and lower bounds on the capacity of the true system are also given in Appendix B. In

the next chapter on simulation results, we demonstrate the accuracy of the truncated system by comparing the eigenvalues of two systems truncated to different lengths. We also compare the capacity calculated for the truncated system to the capacity upper and lower bounds of the true system. The comparisons show that the reduced system is a very accurate one.

In our numerical simulations, we truncate the system to a length, such that for the maximum SNR and the largest spherical volume considered, we have enough eigenmodes to perform the optimal power allocation.

### 3.4 Complete Transmit-Receive System

In Section 2.2, we considered a spherical volume with some arbitrary current distributions  $\mathbf{J}(\mathbf{r}')$  as the input and the radiated electric field  $\mathbf{E}(\mathbf{r})$  in the far-field region as the output. We then analyzed this input-output system mathematically and derived capacity formulas for it. Now, we look at a more realistic complete transmit-receive system which consists of a spherical volume with some arbitrary current distributions as the transmitter, an identical spherical volume having the same size as the receiver and a channel  $\mathbf{H}_{ch}$  connecting the transmitter to the receiver. The described system is shown in Figure 3.1. Let  $\mathbf{J}_1(\mathbf{r}'_1)$  be the input current distributions at the transmitter and  $\mathbf{E}_1(\hat{\mathbf{r}}_1)$  be the radiated electric field in the direction  $\hat{\mathbf{r}}_1$ . Also, let  $\mathbf{J}_2(\mathbf{r}'_2)$  be the current distribution induced at the receiver due to electric field

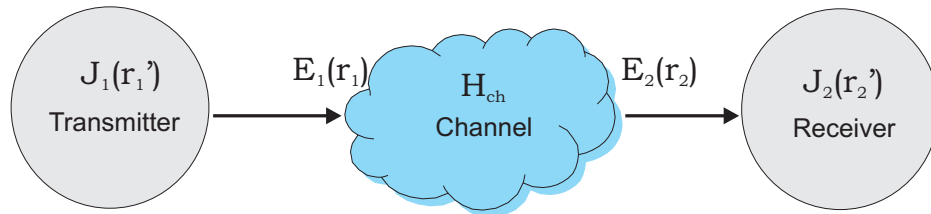


Figure 3.1: Complete Signal Model with Transmitter, Receiver and Channel

$\mathbf{E}_2(\hat{\mathbf{r}}_2)$  from direction  $\hat{\mathbf{r}}_2$ .  $\mathbf{H}_{ch}$  represents the channel matrix connecting electric field intensities between all possible directions  $\hat{\mathbf{r}}_1$  and  $\hat{\mathbf{r}}_2$ . The matrix  $\mathbf{H}_{ch}$  has random entries with the values depending on the channel scattering and fading conditions. For our system, we assume an ideal fully scattered channel and Rayleigh fading conditions. Therefore the channel solid angle  $\Omega$  is  $4\pi$  and the channel matrix  $\mathbf{H}_{ch}$  is  $\mathcal{CN}(\mathbf{0}, \mathbf{I}_{N_t})$ .

Recall the input-output system equation (3.21) derived in Section 3.1.1. Let us rewrite a shorthand notation for it

$$\mathbf{D}^1 = \mathbf{\Gamma} \mathbf{A} \mathbf{C}^1 \quad (3.36)$$

with  $\mathbf{D}^1$  representing the left hand side vector of coefficients  $(D_x, D_y, D_z)^T$ ,  $\mathbf{C}^1$  representing the right hand side vector of coefficients  $(C_x, C_y, C_z)^T$  and  $\mathbf{\Gamma}$ ,  $\mathbf{A}$  having been defined in equation (3.21). Now let us define the coefficient vectors for the discrete representation of the electric field and the current distributions on the receiver side. This discrete representation of the electric field and current distributions in terms of the basis functions and corresponding coefficients can be derived in the same way as was done at the transmitter side, and would give similar results. Let  $\mathbf{C}^2 = (C_x^2, C_y^2, C_z^2)^T$

be the coefficient vector for the electric field and  $\mathbf{D}^2 = (D_x^2, D_y^2, D_z^2)^T$  be the coefficient vector for current distributions at the receiver side. Then from the reciprocity theorem for antennas [21], we have the input-output equation at the receiver side

$$\mathbf{C}^2 = (\mathbf{\Gamma A})^\dagger \mathbf{D}^2 \quad (3.37)$$

Let us now incorporate the channel matrix  $\mathbf{H}_{ch}$  introduced due to scattering in the environment to derive the input-output equation for the complete system starting at the transmitting volume and terminating at the receiving volume. The electric field at the receiver side and the electric field at the transmitter side are related by

$$\mathbf{D}^2 = \mathbf{H}_{ch} \mathbf{D}^1 \quad (3.38)$$

Now, using equations (3.36), (3.37) and (3.38) we can write the input-output equation for the complete system as

$$\begin{aligned} \mathbf{C}^2 &= (\mathbf{\Gamma A})^\dagger \mathbf{H}_{ch} (\mathbf{\Gamma A}) \mathbf{C}^1 \\ \Rightarrow \mathbf{C}^2 &= \mathbf{H}_{new} \mathbf{C}^1 \end{aligned} \quad (3.39)$$

with  $\mathbf{C}^1$  representing the discrete equivalent of current distributions on the transmitter side,  $\mathbf{C}^2$  representing the discrete equivalent of current distributions on the receiver side, and  $\mathbf{H}_{new} = (\mathbf{\Gamma A})^\dagger \mathbf{H}_{ch} (\mathbf{\Gamma A})$  being the matrix connecting the two.

### 3.4.1 Capacity Calculations and Normalization for the Complete System

With the current distributions at the transmitting volume being the input and the current distributions induced at the receiving volume being the output of our complete system, we derived the input-output relation in equation (3.39). Now that we have the input-output relation in the form of a MIMO system described in Section 3.2, we can find the capacity for this system. Let us rewrite the MIMO system equation

$$\mathbf{y} = k\sqrt{\frac{P}{N_t}}\mathbf{H}\mathbf{x} + \mathbf{n} \quad (3.40)$$

with  $k$  being the normalization constant which we determine next and the channel matrix  $\mathbf{H}$  being equal to  $\mathbf{H}_{new} = (\mathbf{\Gamma}\mathbf{A})^\dagger\mathbf{H}_{ch}(\mathbf{\Gamma}\mathbf{A})$  for this system. The channel capacity formulas remain the same as described previously with the only change being the new channel matrix  $\mathbf{H}_{new}$ . Reiterating the capacity formulas, we have for the NCSI case,

$$C = \mathcal{E} \left[ \sum_{i=1}^r \log_2 \left( 1 + k^2 \frac{P}{N_t} \lambda_i \right) \right] \quad (3.41)$$

and for the CSI case,

$$C = \mathcal{E} \left[ \sum_{i=1}^{n^*} \log_2 \left( \mu \frac{k^2 P}{N_t} \lambda_i \right) \right] \quad (3.42)$$

with  $r$  being the rank of matrix  $\mathbf{H}_{new}$ ,  $(\lambda_1, \dots, \lambda_r)$  the positive eigenvalues of  $\mathbf{H}_{new}\mathbf{H}_{new}^\dagger$ ,  $n^*$  the number of eigenmodes getting positive power and  $\mu$  a constant satisfying  $\sum_{i=1}^{n^*} \left( \mu - \frac{N_t}{k^2 P \lambda_i} \right) = N_t$

## Normalization

Again, the normalization constant  $k$  needs to be defined appropriately to be able to interpret the results that we get using the capacity formulas. Recall that in Section 3.2, we had defined a baseline system and then calculated the normalization constant  $k$  such that we get a SNR of  $P$  at the receiver. We then used the same normalization constant for systems with different radii  $a$  in order to capture the capacity increase purely due to increase in size of the transmitter. For the more realistic complete transmit-receive system, we are interested in seeing if the results on capacity and the spatial degrees of freedom would follow the same trends as observed for the previous system. Therefore, we calculate the normalization constant in the same way as was calculated for the previous system, which is given by

$$k = \frac{\sqrt{N_t N_r}}{\sqrt{\text{Tr}\{\mathcal{E}(\mathbf{H}_{new} \mathbf{H}_{new}^\dagger)\}}} \quad (3.43)$$

We can now use this new normalization constant  $k$  to calculate and compare the capacities for the complete system.

In this chapter we started by reducing the continuous-time system to its discrete-time equivalent. We then used the discrete-time equivalent system to derive the formulas for capacity and spatial degrees of freedom. We also formulated a complete transmit-receive system and analyzed it. Now we move on to numerical simulations which are presented in the next chapter.

## Chapter 4

# Simulation Results

In this chapter, we use numerical simulations to look at the behavior of the following. First, we look at the error caused due to system truncation by comparing eigenvalues for two different systems. Then, we look at the spatial degrees of freedom and how they vary with the size of the spherical volume and SNR. Next, we look at capacity calculations and analyze its variations with the size of the spherical volume and SNR. We then look at the gains in capacity and spatial degrees of freedom that can be achieved by using 3-d input current distributions instead of 1-d current distributions. We also compare the calculated capacity with the capacity upper and lower bounds to verify the accuracy of the truncated system. Finally, we give simulation results for the complete transmit-receive system.

We point out here that the radius of the spherical volume  $a$  used throughout this

thesis has been normalized with respect to the wavelength  $\lambda$ . Therefore  $a = 1$  would mean that the spherical volume has a radius of  $1\lambda$ . We use this notation in this chapter as well.

## 4.1 Error Due to System Truncation

Here, we will look at the error caused due to truncation of our infinite-dimensional system to a finite-dimensional one. To this end, we compare the eigenvalues of two systems truncated to different lengths. The first system is truncated such that the size of the  $\mathbf{H} = \mathbf{\Gamma}\mathbf{A}$  matrix is  $1875 \times 1875$ . The second system is truncated such that  $\mathbf{\Gamma}\mathbf{A}$  is a  $2700 \times 2700$  matrix. Figure 4.1 plots the first 1000 eigenvalues for the two systems described above and having a radius of 1. Similarly, Figure 4.2 plots the first 1000 eigenvalues for the two systems having a radius of 3. In Figure 4.3, we also plot the difference in eigenvalues of the two systems truncated to different lengths. The figure gives the error plots for the radius varying from 0.5 to 3. The three figures tend to suggest that for a sufficiently large size of the  $\mathbf{\Gamma}\mathbf{A}$  matrix, the error due to truncation is small and the truncated system is converging to the true continuous-time system. From Figure 4.3, we note that for the largest sized spherical volume considered here, the maximum error in eigenvalues is on the order of  $10^{-7}$  which is extremely small. Since the  $1875 \times 1875$  has an extremely small error, we will use this system for simulations hereafter.

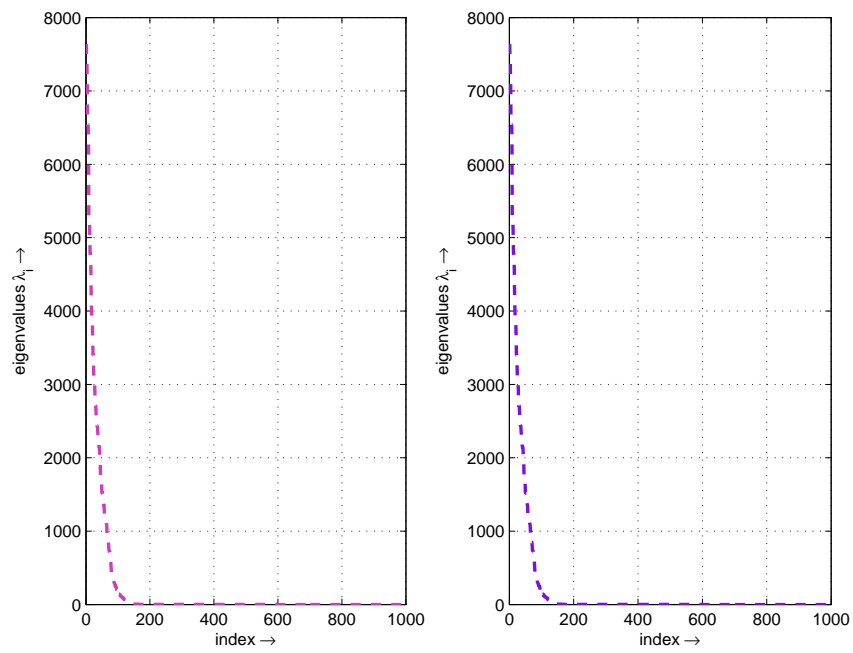


Figure 4.1: First 1000 eigenvalues for systems truncated to lengths of 1875 and 2700 respectively, and radius  $a = 1$

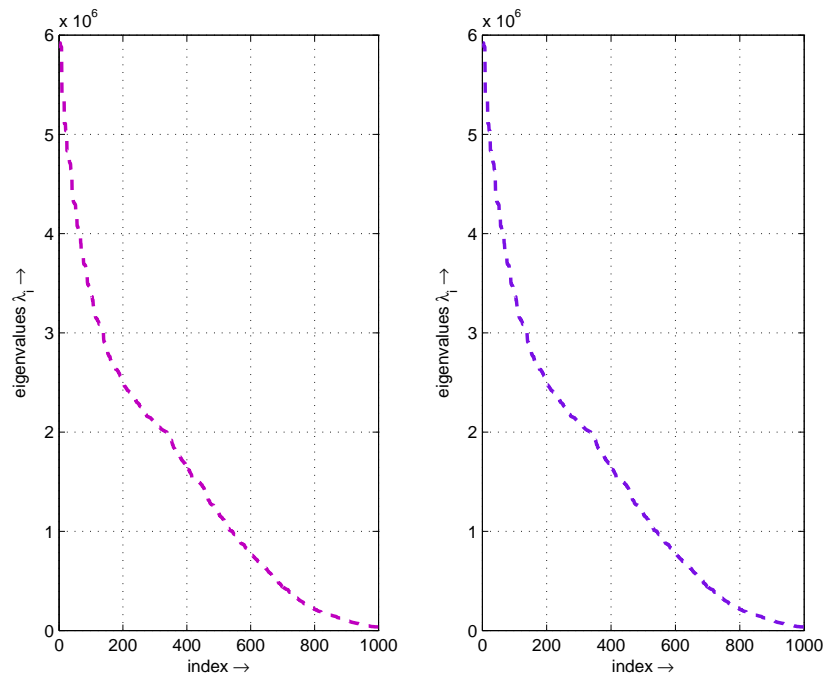


Figure 4.2: First 1000 eigenvalues for systems truncated to lengths of 1875 and 2700 respectively, and radius  $a = 3$

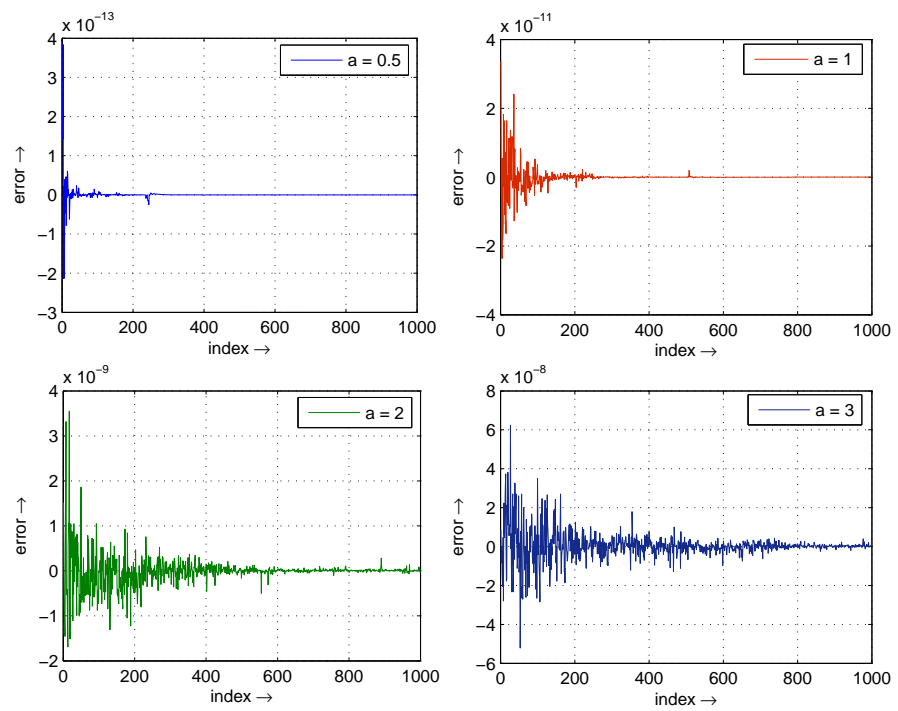


Figure 4.3: Difference in eigenvalues for systems truncated to lengths of 1875 and 2700, and radius  $a$  varying from 0.5 to 3

## 4.2 Spatial Degrees of Freedom

In this section we will look at the behavior of the spatial degrees of freedom with respect to the size of the input spherical volume and the SNR. First, we look at how the spatial degrees of freedom  $n^*$ , vary with the size of the input spherical volume. To this end, we plot two figures. The first one, i.e. Figure 4.4 plots  $n^*$  for the 3-d input current distributions (denoted by  $n^*(3\text{-d})$  here) against the wavevector-aperture product  $\mathcal{A}|\Omega| = 4\pi^2 a^2$  for fixed SNR's and radius  $a$  varying from 0.5 to 3. The two plots in the figure are calculated at SNR's 20 dB and 0 dB respectively. Similarly, Figure 4.5 plots  $n^*(1\text{-d})$  for 1-d input current distributions. The two figures suggest that the spatial degrees of freedom  $n^*$  have a linear relationship with the effective aperture  $\mathcal{A} = \pi a^2$  of the input spherical volume.

Earlier in Section 3.3, we had mentioned an upper bound on the spatial degrees of freedom that has been claimed by Poon *et al.* in [8]. The claim in [8] is that for spherical arrays, the wavevector-aperture product  $\mathcal{A}|\Omega| = 4\pi^2 a^2$  forms an upper bound on  $n^*(1\text{-d})$ . Here, our simulation results tend to show that although  $n^*(1\text{-d})$  follows a linear relationship with  $4\pi^2 a^2$  (Figure 4.5), the factor of scaling could be more than one making  $n^*(1\text{-d})$  greater than  $4\pi^2 a^2$ . Table 4.1 gives the ratio  $n^*(1\text{-d})/4\pi^2 a^2$ , for SNR varying from 0 dB to 20 dB and the radius varying from 0.5 to 3.

It can be seen from the table that  $n^*(1\text{-d})$  is varying between 1.3 to 2 times  $4\pi^2 a^2$  for different values of the radius and SNR's considered here. Although the results we

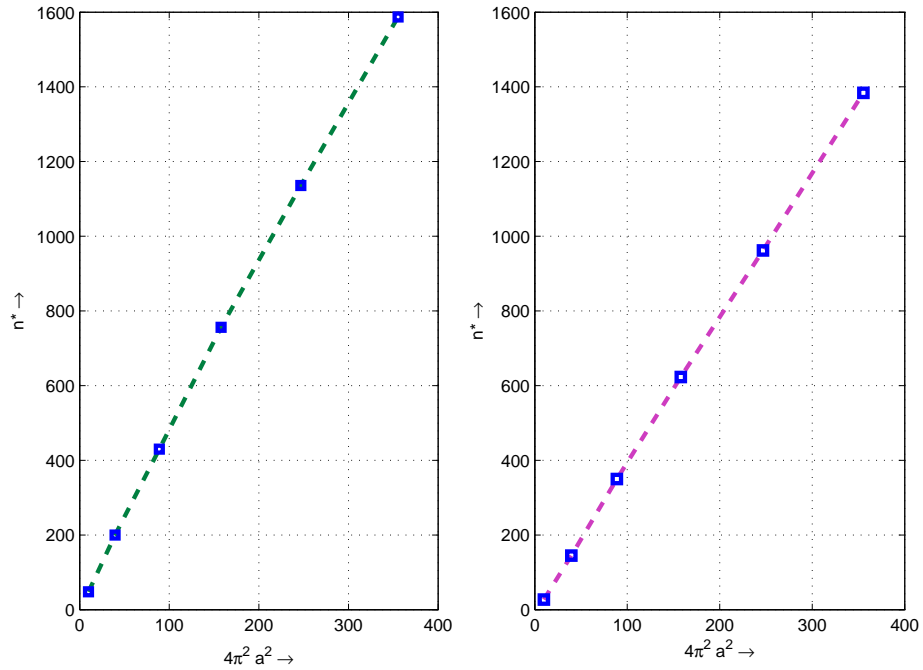


Figure 4.4: Plot of  $n^*(3-d)$  vs.  $4\pi^2 a^2$  at SNR's of 20 dB and 0 dB respectively

Table 4.1: Ratio  $n^*(1-d)/4\pi^2 a^2$  for different SNR values and radius of the spherical volume

SNR (dB)	Radius ( $a$ )					
	0.5	1	1.5	2	2.5	3
0 dB	1.31	1.39	1.36	1.42	1.41	1.36
4 dB	1.62	1.62	1.53	1.42	1.46	1.38
8 dB	1.62	1.62	1.62	1.53	1.46	1.48
12 dB	1.62	1.62	1.62	1.62	1.48	1.48
16 dB	1.62	1.62	1.62	1.62	1.61	1.48
20 dB	1.82	2.00	1.81	1.62	1.62	1.58

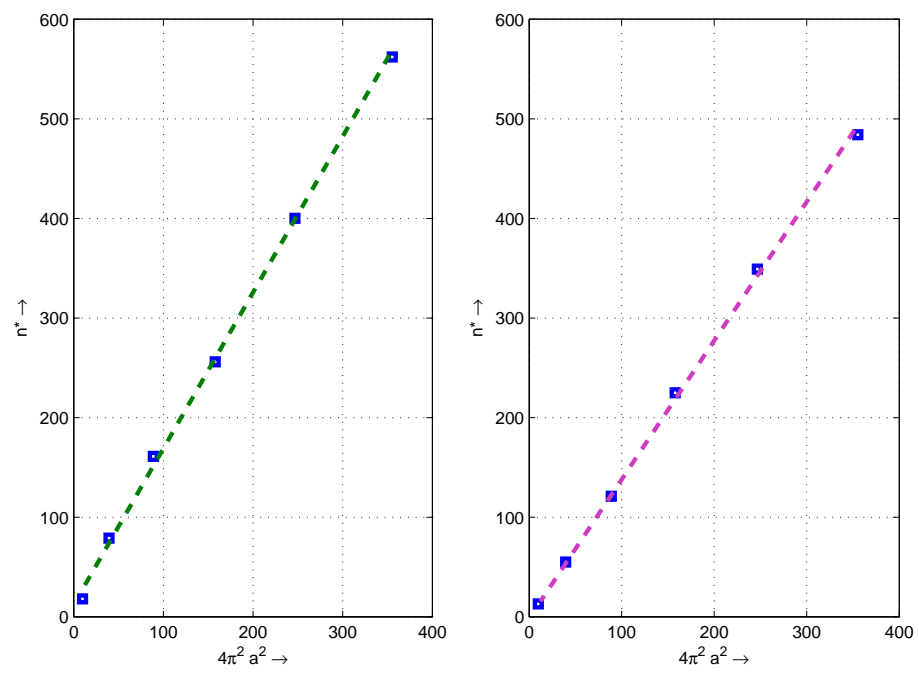


Figure 4.5: Plot of  $n^*(1-d)$  vs.  $4\pi^2 a^2$  at SNR's of 20 dB and 0 dB respectively

Table 4.2: Spatial Degrees of Freedom  $n^*(1-d)$  for different SNR values and radius of the spherical volume

SNR (dB) \ Radius ( $a$ )	0.5	1	1.5	2	2.5	3
0 dB	13	55	121	225	349	484
4 dB	16	64	136	225	361	492
8 dB	16	64	144	242	361	527
12 dB	16	64	144	256	367	529
16 dB	16	64	144	256	398	529
20 dB	18	79	161	256	400	562

have are not sufficient to exactly determine the ratio  $n^*(1-d)/4\pi^2a^2$  based on a given radius and SNR, the results suggest that the number of spatial degrees of freedom are not restricted to  $4\pi^2a^2$ .

In Section 3.3, we mentioned that we expect  $n^*$  to increase with SNR as well and gave an intuitive reason for it. Here, we give the results for  $n^*(1-d)$  in table 4.2. The table gives  $n^*(1-d)$  for SNR varying from 0 dB to 20 dB and radius  $a$  varying from 0.5 to 3. The table suggests that for any particular size of the spherical volume, the spatial degrees of freedom continues to increase with SNR as well. However, the rate of increase with SNR seems to be lesser than the rate of increase with size.

### 4.3 Channel Capacity

Now we move to the capacity plots for our system. Here again, we are interested in looking at the behavior of capacity with respect to the SNR and the size of the

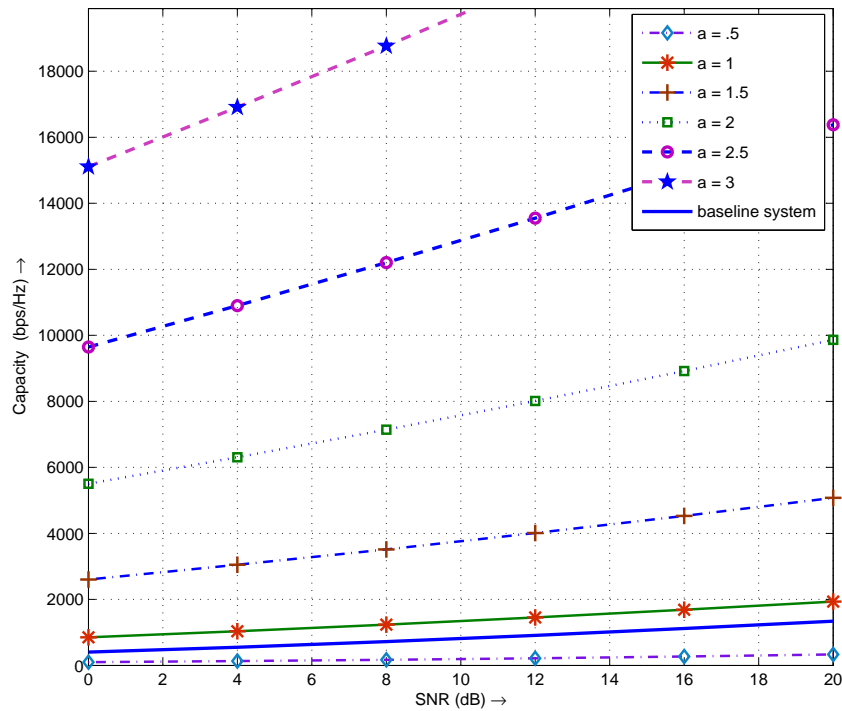


Figure 4.6: Capacities vs. SNR for 3-d input current distributions and  $a$  varying from 0.5 to 3

spherical volume. First, we look at the variation in capacity with SNR. To this end, we plot the capacity against SNR for a system having 3-d input current distributions in Figure 4.6. The figure gives plots for the radius  $a$  varying from 0.5 to 3. Similarly, we give the capacity plots for 1-d input current distributions in Figure 4.7. The two figures tend to suggest that capacity values for the continuous-time system are increasing linearly with the SNR in dB i.e.  $C \propto \log(\text{SNR})$ .

From the figures, we also notice that the capacity values are extremely high, on the order of thousands of bps/Hz for high SNR. However, the reason for such high values

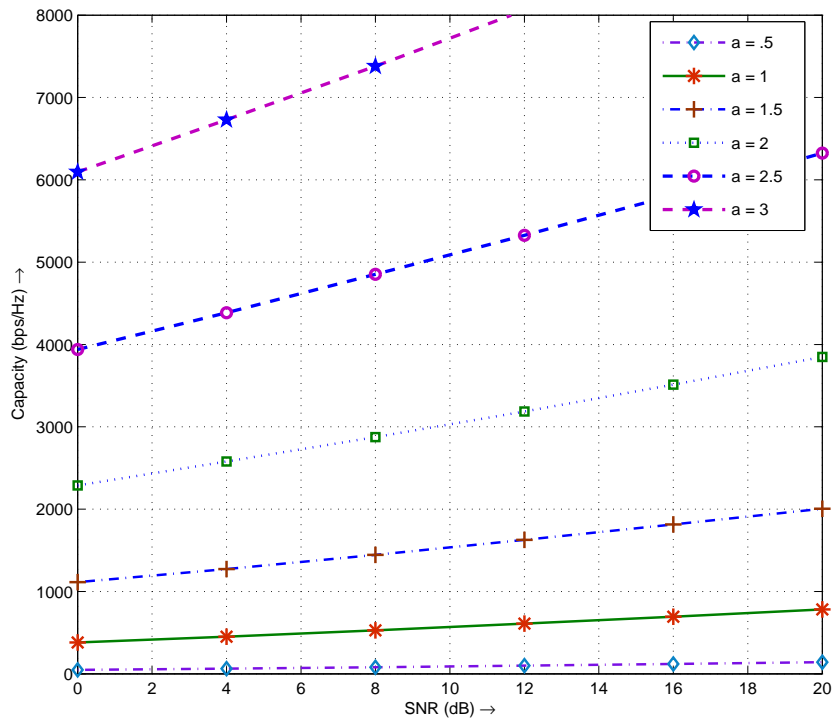


Figure 4.7: Capacities vs. SNR for 1-d input current distributions with  $a$  varying from 0.5 to 3

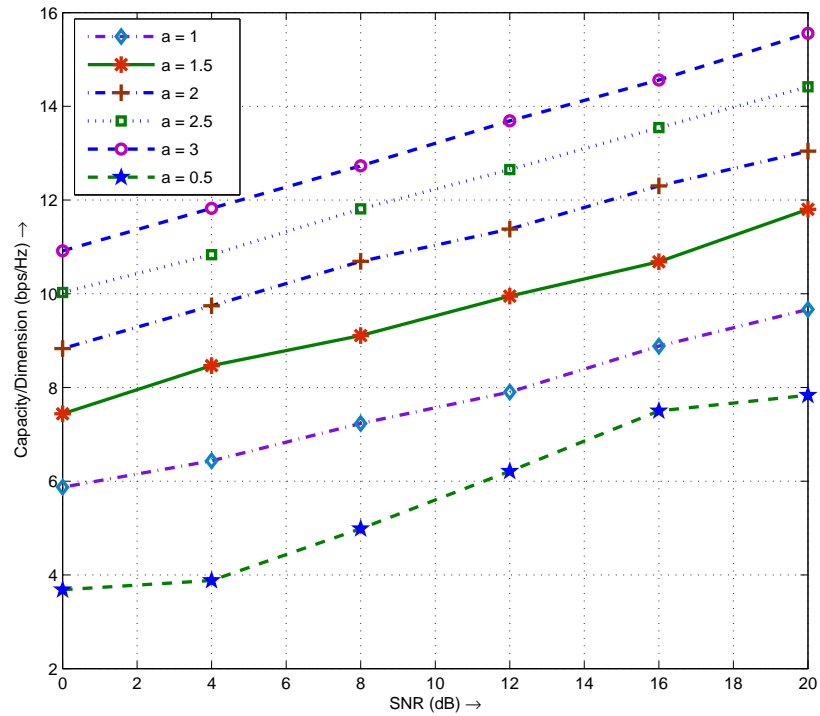


Figure 4.8: Capacity/Dimension vs. SNR for 3-d input current distributions with  $a$  varying from 0.5 to 3

is that the spatial degrees of freedom are also very high, on the order of hundreds. Therefore, we also plot the capacities per signalling dimension in Figure 4.8 for 3-d input current distributions which show the capacity values per dimension to be around 3-15 bps/Hz which is comparable to the capacity per signalling dimension achieved over AWGN SISO channels.

Next, we look at the variation in capacity with the size of the spherical volume. To this end, we plot the capacity values against the wavevector-aperture product  $\mathcal{A}|\Omega| = 4\pi^2 a^2$  in Figure 4.9 with the radius of the spherical volume varying from 0.5

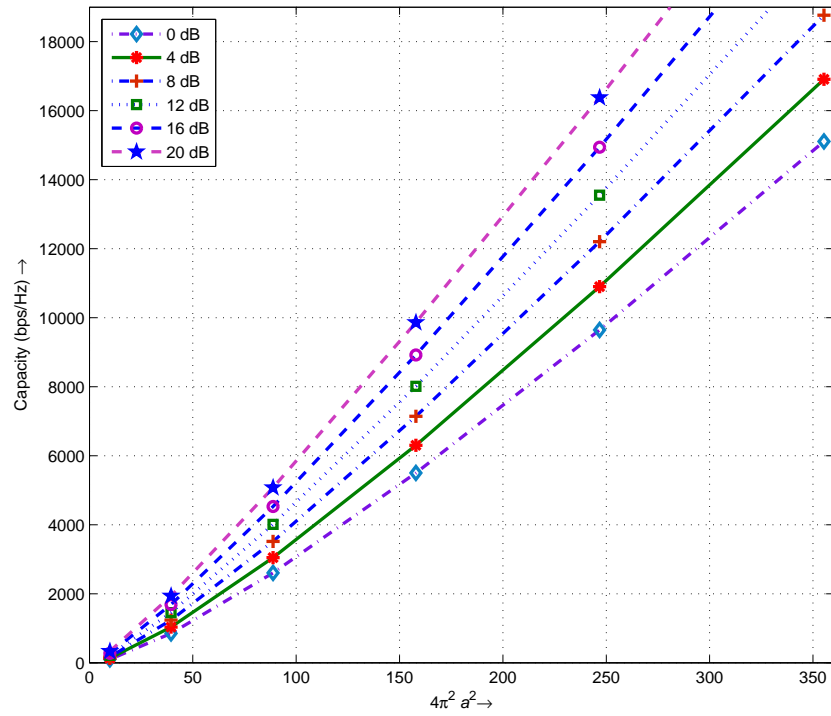


Figure 4.9: Capacity vs.  $4\pi^2 a^2$  with SNR varying from 0 dB to 20 dB

to 3. The different plots in the figure give capacity results for SNR varying from 0 dB to 20 dB. In this case, the figure tends to show a faster than linear rate of increase in capacity with the effective aperture  $\mathcal{A}$  of the spherical volume. Our simulation results suggest that the capacity  $C$  seems to be proportional to  $(\mathcal{A})^c$  with the value of  $c$  varying between 1.1 and 1.3.

## 4.4 Increase in Capacity and Spatial Degrees of Freedom on using 3-d Current Distributions

In this section, we look at the important aspect of the gain in capacity and spatial degrees of freedom that can be achieved by using 3-d current distributions (or tri-polarized antennas) instead of using 1-d current distributions (or uni-polarized antennas). Here again, we compare our simulation results with the claim in [8] that says that we could only achieve a maximum capacity gain of two times by using 3-d current distributions instead of 1-d current distributions.

First, in Figure 4.10 we plot the ratio of capacities  $C(3\text{-d})/C(1\text{-d})$  for systems with 3-d input current distributions relative to systems with 1-d input current distributions against the radius of the spherical volume at SNR's of 0 dB and 20 dB respectively. The figure suggests a monotonic increase in the capacity ratio with size which seems to be approaching an asymptote. The ratio is around 2.6 for  $a = 3$  and SNR of 20 dB and we conjecture that for a sufficiently large input spherical volume, we could get a capacity gain upto a factor of 3 times by using 3-d current distributions instead of 1-d current distributions. The figure also suggests an increase in the capacity ratio with SNR.

Next, we look at the ratio,  $n^*(3\text{-d})/n^*(1\text{-d})$  of the spatial degrees of freedom due to 3-d current distributions relative to the spatial degrees of freedom due to 1-d input

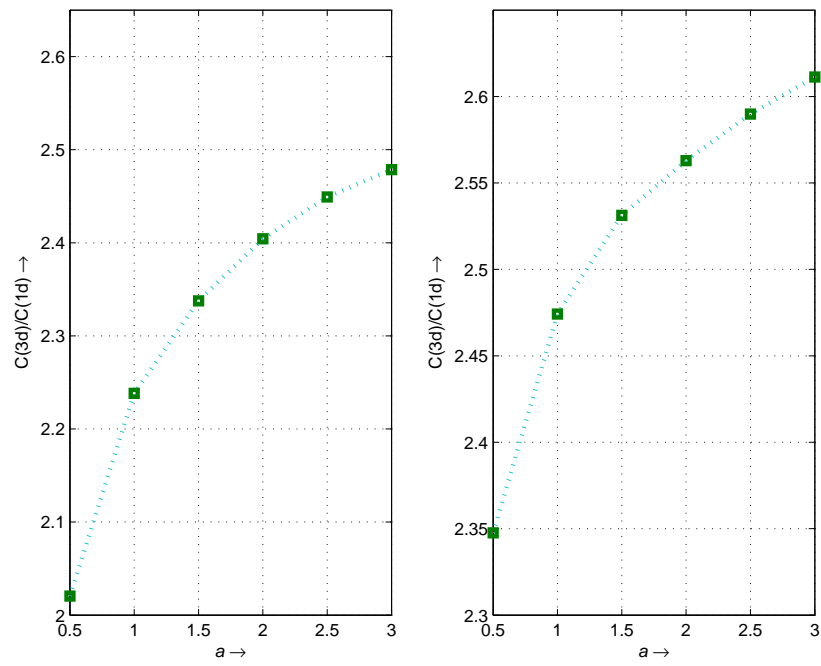


Figure 4.10: Capacity Ratio  $C(3-d)/C(1-d)$  vs.  $a$  for SNR's of 0db and 20db respectively

current distributions. To this end, Figure 4.11 plots the ratio  $n^*(3-d)/n^*(1-d)$  against the radius of the spherical volume at SNR's of 0 dB and 20 dB respectively. Here, we notice that the ratio of spatial degrees of freedom does not seem to follow a monotonic increase with size or SNR. Since in our system, there are sets of eigenvalues having almost identical values within a set, the water-pouring algorithm would allocate power to all values in a set simultaneously, causing a sudden jump in the spatial degrees of freedom. This behavior of the spatial degrees of freedom can also be noted in Table 4.2. These jumps in the number of spatial degrees of freedom for the two systems seem to be the reason for the variations in the ratio  $n^*(3-d)/n^*(1-d)$ . Despite these variations, we see that the ratio is between 2-2.8 for the different radius and SNR's considered here. Based on these results, we would again expect the ratio to go 3 for a sufficiently large spherical volume and at high SNR's. On the other extreme, we also expect this ratio to be 1 for a sufficiently small spherical volume, since there would be only one significant eigenmode which is used for transmission, regardless of the current distributions being 1-d or 3-d.

## 4.5 Impact of Truncation on Capacity

As we mentioned in Section 3.2, we now compare the capacity results with the capacity lower and upper bounds (equation B.5) defined in Appendix B to look at the impact of the truncation error on capacity calculations. Figure 4.12 plots the

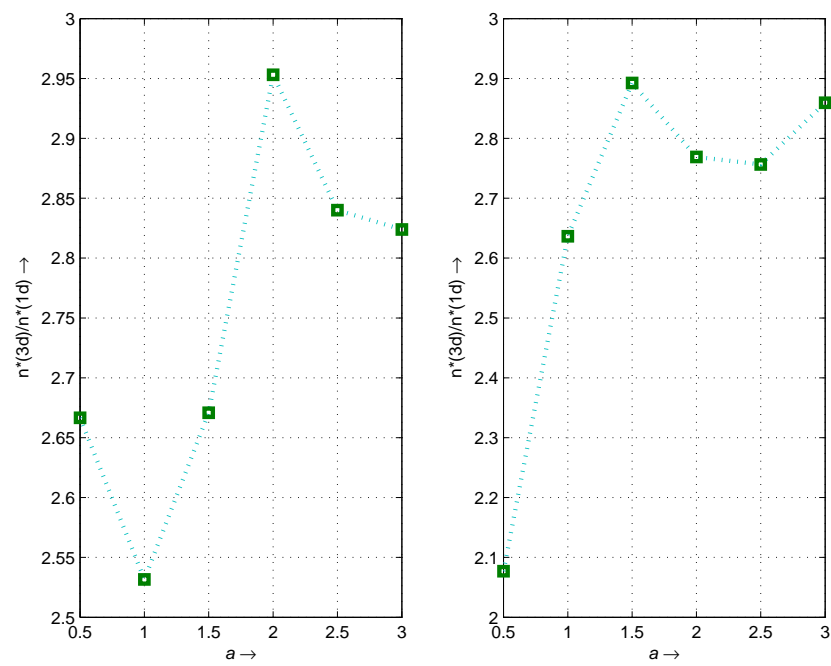


Figure 4.11: Ratio  $n^*(3-d)/n^*(1-d)$  vs.  $a$  for SNR's of 0 dB and 20 dB respectively

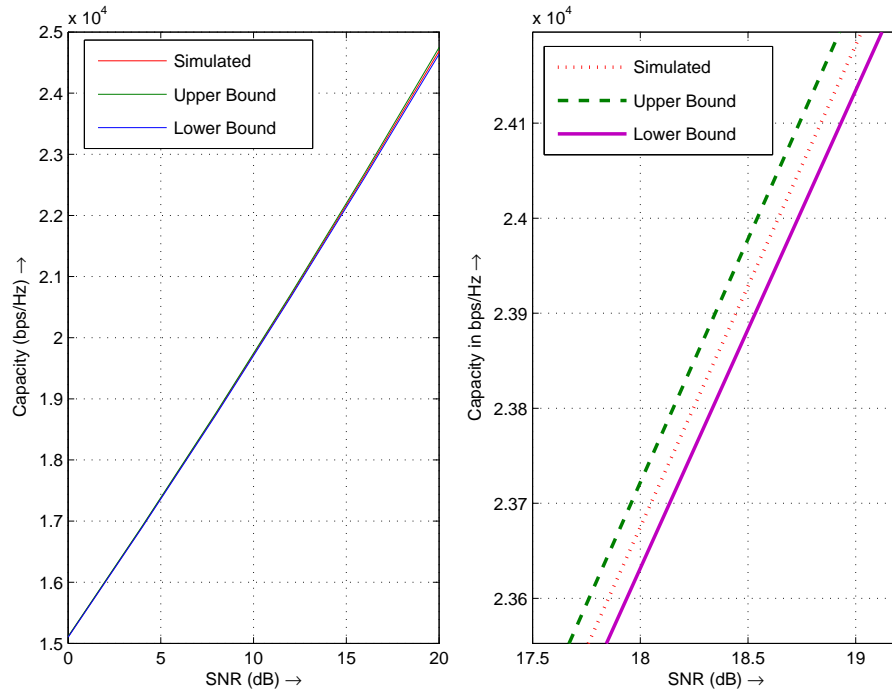


Figure 4.12: Capacity bounds and calculated capacity vs. SNR for  $a = 3$ .

calculated capacity along with the capacity bounds vs. the SNR. The capacity lower and upper bounds are calculated using the water-pouring algorithm on the eigenvalue sets defined in (B.3) and (B.4) respectively. It can be seen from the figure that the calculated capacity is almost identical to capacity bounds for low SNR's with the error in capacity increasing slightly at high SNR's. However the capacity results are still very accurate with the error being around 0.1 dB at an SNR of 18 dB as seen in the enlarged version of the error plot.

## 4.6 Results for the Complete Transmit-Receive System

Earlier in Section 3.4, we had introduced a receiving spherical volume along with the channel scattering matrix to our system model to define a more realistic complete transmit-receive system. The capacity formulations were then derived for the new system along with appropriate expression for the normalization constant. In this section we look at the results on the capacity and spatial degrees of freedom for the complete system and see if they follow the same trends as were observed for our previous system. For our calculations, we assume an ideal fully scattered channel and Rayleigh fading conditions. Therefore the channel solid angle  $\Omega$  is  $4\pi$  and the channel matrix  $\mathbf{H}_{ch}$  is  $\mathcal{CN}(\mathbf{0}, \mathbf{I}_{N_t})$ .

First, we plot the spatial degrees of freedom,  $n^*(3\text{-d})$  and  $n^*(1\text{-d})$  for 3-d and 1-d current distributions against the wavevector-aperture product  $\mathcal{A}|\Omega| = 4\pi^2 a^2$  in Figures 4.13 and 4.14 respectively. The two figures suggest that as for the previous system, the spatial degrees of freedom for the complete system increase linearly with the effective aperture of the spherical volume.

Next, we give the capacity vs. SNR plots of the complete system for 3-d and 1-d input current distributions in Figures 4.15 and 4.16 respectively. The capacity plots are given for the radius of the transmitter and receiver volumes varying from 0.5 to

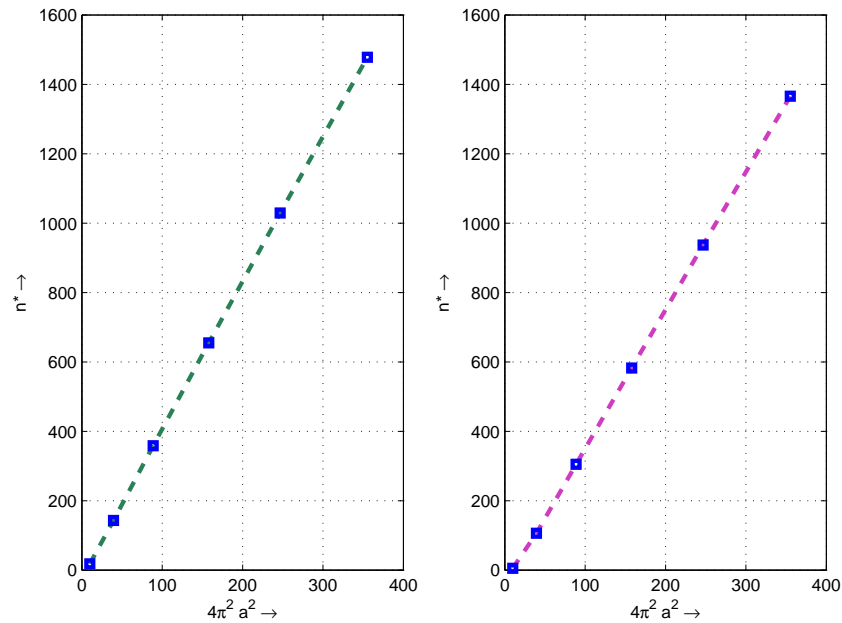


Figure 4.13: Plot of  $n^*(3\text{-d})$  vs.  $4\pi^2 a^2$  for the complete system at SNR's of 20 dB and 0 dB respectively

3. Here again, the plots suggest a linear relationship between capacity and the SNR in dB, i.e.  $C \propto \log(\text{SNR})$ .

In Figure 4.17, we plot the capacity values against  $\mathcal{A}|\Omega|$  for SNR varying from 0 dB to 20 dB. Again, we see a slightly faster than linear growth in capacity values with the effective aperture of the spherical volume.

Finally in Figure 4.18, we plot the capacity ratio  $C(3\text{-d})/C(1\text{-d})$  against the radius of the spherical volume to observe the gains in capacity achieved on using 3-d current distributions relative to 1-d current distributions. The two plots in the figure are at SNR's of 0 dB and 20 dB respectively. Although the gains achieved for this system

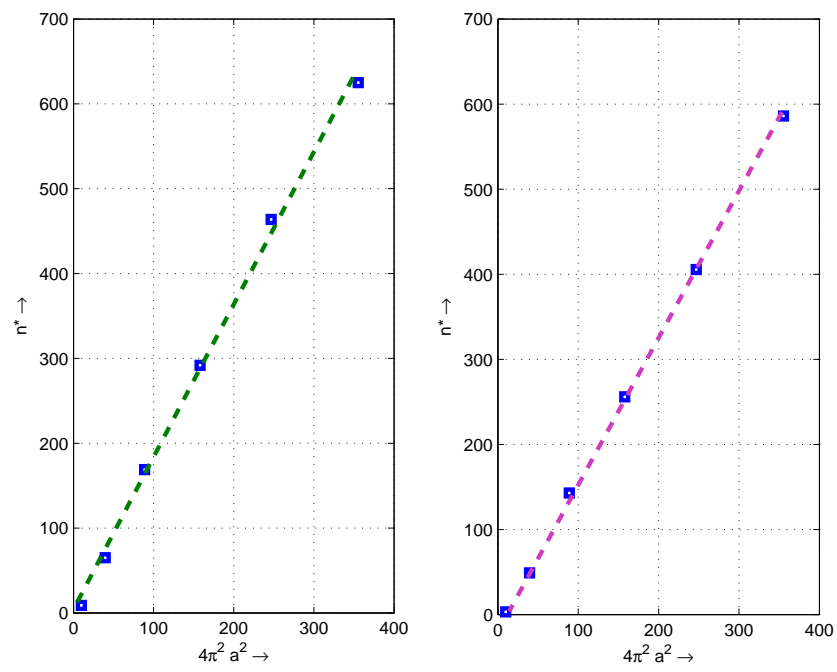


Figure 4.14: Plot of  $n^*(1-d)$  vs.  $4\pi^2 a^2$  for the complete system at SNR's of 20 dB and 0 dB respectively

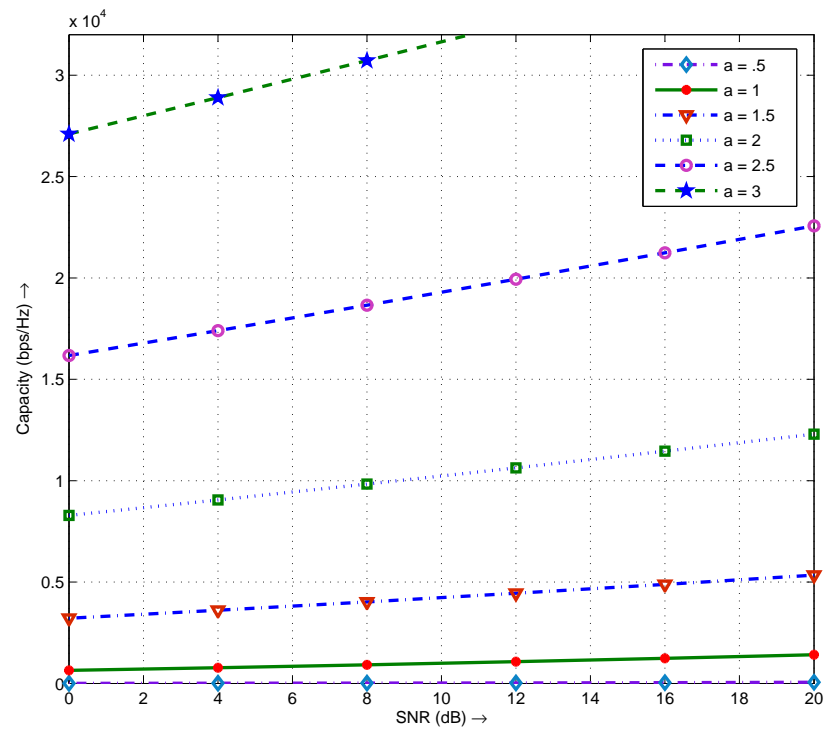


Figure 4.15: Capacities vs. SNR for the complete system with 3-d input current distributions and  $a$  varying from 0.5 to 3

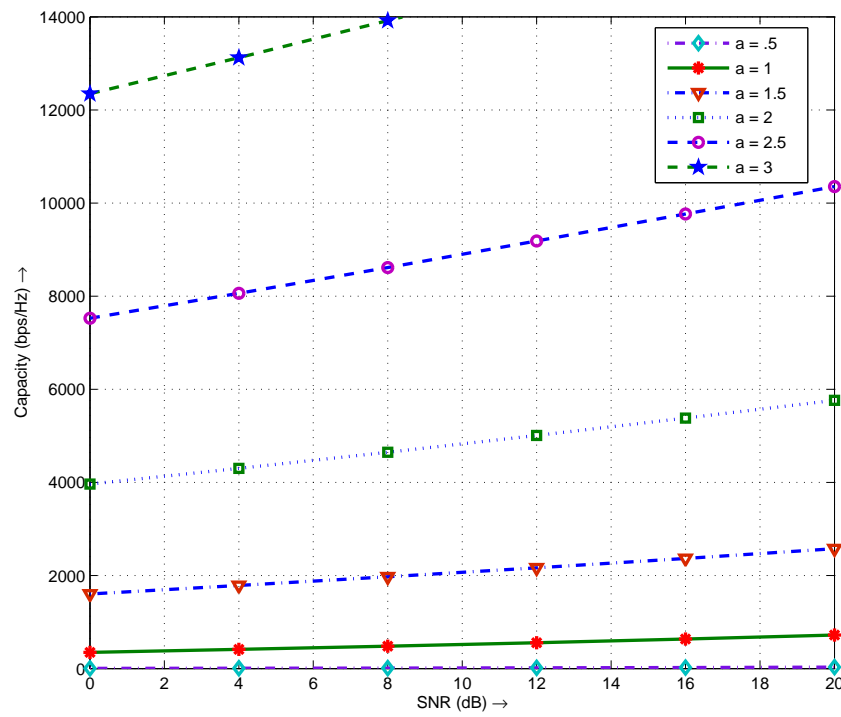


Figure 4.16: Capacities vs. SNR for the complete system with 1-d input current distributions and  $a$  varying from 0.5 to 3

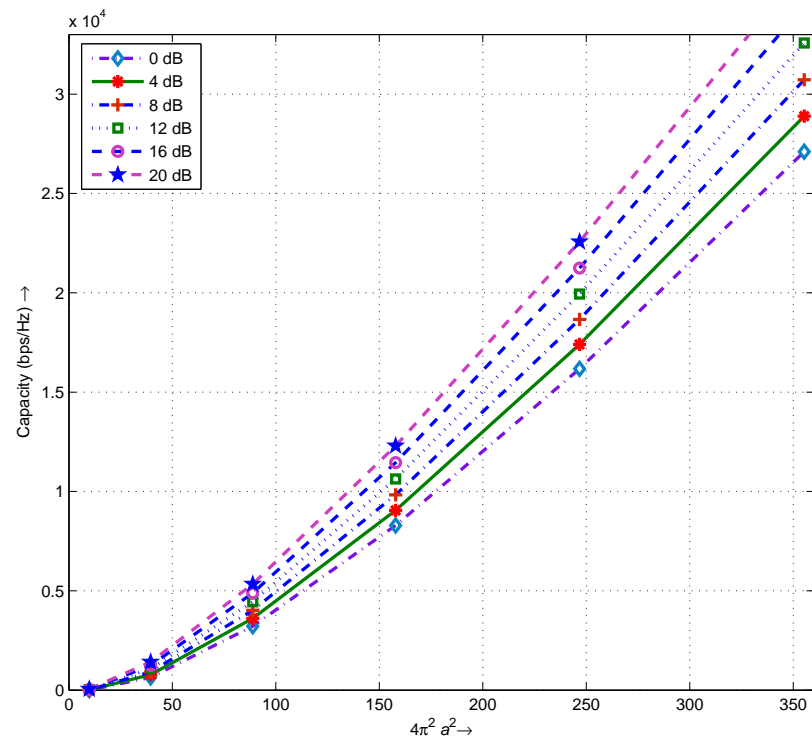


Figure 4.17: Capacity vs.  $4\pi^2 a^2$  for the complete system and SNR varying from 0 dB to 20 dB

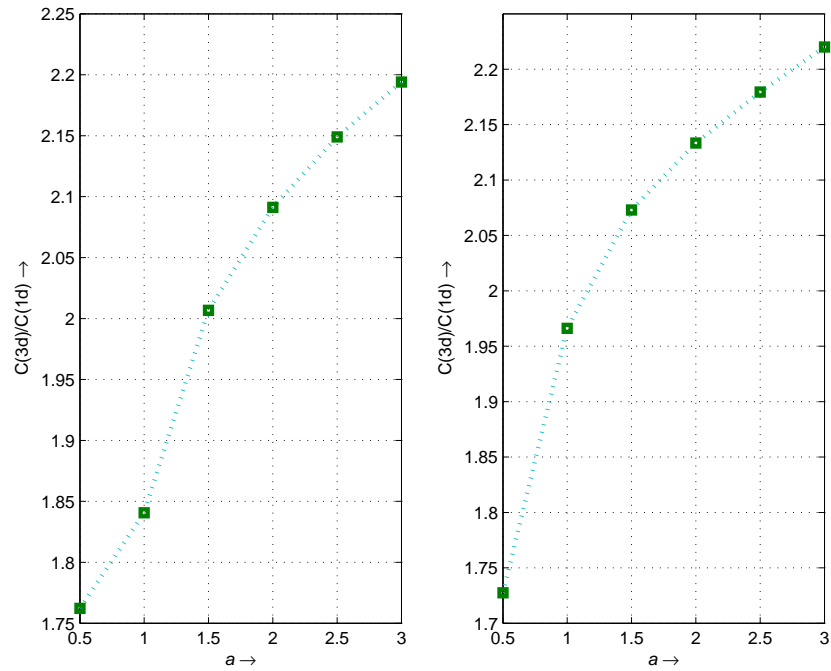


Figure 4.18: Capacity Ratio  $C(3-d)/C(1-d)$  vs.  $a$  for the complete system at SNR's 0db and 20db respectively

(1.7-2.3) seem to be slightly lesser as compared to the previous system (2-2.6), we still observe the same trends i.e. the capacity ratio seems to be increasing monotonically to an asymptote, which we conjecture to be 3 for sufficiently large systems.

In this section we saw that all the trends in capacity values and spatial degrees of freedom that were observed for our previous system, seem to carry over to a more realistic complete transmit-receive system also.

## Chapter 5

# Conclusions

We now provide a summary of the results and also offer some pointers to open problems that can be looked at in future.

We started this thesis by pointing out that at high SNR's, the capacity for MIMO systems increases linearly with the available spatial degrees of freedom, which in turn scales linearly with the minimum of the number of antennas at the transmitter and the receiver under i.i.d Rayleigh fading conditions and complete channel state information at the receiver. However, the number and location of antennas in particular antenna systems constrains the amount of information-exchange that takes place between the transmitter and receiver through the electromagnetic waves, thus also reducing the achievable capacity and spatial degrees of freedom for the system. To overcome these limitations, we looked at a continuous-time system constrained only by its volume.

We studied a system which consists of a spherical volume at the transmitter having some arbitrary current distributions and radiating an electric field around it. A spherical volume in the far-field of the transmitter capable of capturing all the radiated signals was taken to be the receiver. The current distributions in the spherical volume were considered to be the system input while the radiated electric field in the far-field region was considered to be the system output. The radius of the spherical volume was constrained to be  $a$ , and the total power available at the transmitter was  $P$ . We developed a mathematical model for this continuous-time system using electromagnetic theory and later reduced it to a MIMO system form with a matrix channel connecting the system input to the system output. Once in the MIMO form, we were able to use standard capacity formulas to calculate system capacities. Our numerical simulation results tend to suggest the following

1. The spatial degrees of freedom increase linearly with the effective aperture of the spherical volume  $\mathcal{A} = \pi a^2$ . For the transmitter radiating into the entire surrounding space i.e.  $\Omega = 4\pi$ , the spatial degrees of freedom for the system vary between 1.3 to 2 times the wavevector-aperture product  $\mathcal{A}\Omega = 4\pi^2 a^2$  for different values of the radius and SNR considered in this thesis.
2. Capacity for the system shows a linear growth with the SNR in dB and a slightly faster than linear rate of growth with the effective aperture of the spherical volume. For spherical volumes having a radius on the order of a few wavelengths,

the capacities achieved are on the order of thousands of bps/Hz.

3. For a sufficiently large system, capacity gains upto a factor of 3 can be achieved by using 3-d current distributions at the transmitter instead of 1-d current distributions. For spherical arrays having a radius on the order of a few wavelengths, capacity gains of around 2-2.8 times can be achieved.

Finally, we considered a full transmit-receive system consisting of a spherical volume at the transmitter, an identical spherical volume at the receiver and a channel matrix representing the scattering and fading conditions connecting the two. Here, our simulation results suggest that the more realistic complete transmit-receive system also follows the trends on capacity and spatial degrees of freedom observed by the previous system.

Since such continuous-time systems constrained to a volume are just beginning to be looked at, there are a quite a few open problems that need to be addressed. We just point to some of those. First, it would be good to have an analytical solution to spatial degrees of freedom and capacities as opposed to numerical solutions. Second, other practical channel scattering and fading environments could be considered and their impact on capacities studied. Another interesting problem that needs to be looked at is the optimum number of antennas that should be used given the size constraints on the transmitter and/or receiver to achieve most of the promised capacity. Various other transmitter and receiver geometries could also be studied.

## Appendix A

# Recurrence Relations for Spherical Harmonics

It was mentioned earlier in Section 3.1.1 that we can write  $r_{11}Y_{n,m}$  as

$$r_{11}Y_{n,m} = \sum_{n',m'} \gamma_{11,n'm'}^{n,m} Y_{n',m'}$$

due to recurrence relations. Now we show in detail how this is done for one case. The others can be derived similarly. We will only state the results for the other cases. We

start by giving the recurrence relations [19, pp. 245],

$$\begin{aligned}
\cos \theta Y_{n,m} &= \underbrace{\sqrt{\frac{(n+m)(n-m)}{(2n+1)(2n-1)}}}_{a_{n,m}} Y_{n-1,m} + \\
&\quad \underbrace{\sqrt{\frac{(n+m+1)(n-m+1)}{(2n+1)(2n+3)}}}_{b_{n,m}} Y_{n+1,m} \\
\sin \theta e^{j\varphi} Y_{n,m} &= \underbrace{\sqrt{\frac{(n-m)(n-m-1)}{(2n+1)(2n-1)}}}_{c_{n,m}} Y_{n-1,m+1} + \\
&\quad \underbrace{\sqrt{\frac{(n+m+1)(n+m+2)}{(2n+1)(2n+3)}}}_{d_{n,m}} Y_{n+1,m+1} \\
\sin \theta e^{-j\varphi} Y_{n,m} &= \underbrace{\sqrt{\frac{(n+m)(n+m-1)}{(2n+1)(2n-1)}}}_{e_{n,m}} Y_{n-1,m-1} + \\
&\quad \underbrace{\sqrt{\frac{(n-m+1)(n-m+2)}{(2n+1)(2n+3)}}}_{f_{n,m}} Y_{n+1,m-1}
\end{aligned} \tag{A.1}$$

We can write

$$r_{11} Y_{n,m} = (1 - \sin^2 \theta \cos^2 \varphi) Y_{n,m} = Y_{n,m} - (\sin \theta \cos \varphi)(\sin \theta \cos \varphi) Y_{n,m} \tag{A.2}$$

From the recurrence relations, we get

$$2 \sin \theta \cos \varphi Y_{n,m} = c_{n,m} Y_{n-1,m+1} + d_{n,m} Y_{n+1,m+1} + e_{n,m} Y_{n-1,m-1} + f_{n,m} Y_{n+1,m-1} \tag{A.3}$$

$$\begin{aligned}
\Rightarrow \quad 4 \sin^2 \theta \cos^2 \varphi Y_{n,m} &= c_{n,m} 2 \sin \theta \cos \varphi Y_{n-1,m+1} + d_{n,m} 2 \sin \theta \cos \varphi Y_{n+1,m+1} + \\
&\quad e_{n,m} 2 \sin \theta \cos \varphi Y_{n-1,m-1} + f_{n,m} 2 \sin \theta \cos \varphi Y_{n+1,m-1}
\end{aligned} \tag{A.4}$$

Reapplying (A.3) to (A.4) and substituting in (A.2), we get

$$\begin{aligned}
r_{11}Y_{n,m} &= \sum_{n',m'} \gamma_{11,n'm'}^{n,m} Y_{n',m'} \\
&= [(-1/4)e_{n,m}e_{n-1,m-1}] Y_{n-2,m-2} + \\
&\quad [(-1/4)c_{n,m}e_{n-1,m+1} + e_{n,m}c_{n-1,m-1}] Y_{n-2,m} + \\
&\quad [(-1/4)c_{n,m}c_{n-1,m+1}] Y_{n-2,m+2} + \\
&\quad [(-1/4)e_{n,m}f_{n-1,m-1} + f_{n,m}e_{n+1,m-1}] Y_{n,m-2} + \\
&\quad [1 - (1/4)c_{n,m}f_{n-1,m+1} + d_{n,m}e_{n+1,m+1} + \\
&\quad \quad e_{n,m}d_{n-1,m-1} + f_{n,m}c_{n+1,m-1}] Y_{n,m} + \\
&\quad [(-1/4)c_{n,m}d_{n-1,m+1} + d_{n,m}c_{n+1,m+1}] Y_{n,m+2} + \\
&\quad [(-1/4)f_{n,m}f_{n+1,m-1}] Y_{n+2,m-2} + \\
&\quad [(-1/4)d_{n,m}f_{n+1,m+1} + f_{n,m}d_{n+1,m-1}] Y_{n+2,m} + \\
&\quad [(-1/4)d_{n,m}d_{n+1,m+1}] Y_{n+2,m+2}
\end{aligned} \tag{A.5}$$

From (A.5), we get the  $\gamma$  coefficients for the  $\Gamma_{11}$  matrix. Following a similar procedure we can find the  $\gamma$  coefficients for the other  $\Gamma$  matrices also. We now state the coefficient

values for the other matrices. For the  $\Gamma_{12}$  matrix, we have

$$\begin{aligned}
\gamma_{12(n-2,m-2)} &= (1/4i)(-e_{n,m}e_{n-1,m-1}) \\
\gamma_{12(n-2,m)} &= (1/4i)(-c_{n,m}e_{n-1,m+1} + e_{n,m}c_{n-1,m-1}) \\
\gamma_{12(n-2,m+2)} &= (1/4i)(c_{n,m}c_{n-1,m+1}) \\
\gamma_{12(n,m-2)} &= (1/4i)(-e_{n,m}f_{n-1,m-1} - f_{n,m}e_{n+1,m-1}) \\
\gamma_{12(n,m)} &= (1/4i)(-c_{n,m}f_{n-1,m+1} - d_{n,m}e_{n+1,m+1} + \\
&\quad e_{n,m}d_{n-1,m-1} + f_{n,m}c_{n+1,m-1}) \\
\gamma_{12(n,m+2)} &= (1/4i)(c_{n,m}d_{n-1,m+1} + d_{n,m}c_{n+1,m+1}) \\
\gamma_{12(n+2,m-2)} &= (1/4i)(-f_{n,m}f_{n+1,m-1}) \\
\gamma_{12(n+2,m)} &= (1/4i)(-d_{n,m}f_{n+1,m+1} + f_{n,m}d_{n+1,m-1}) \\
\gamma_{12(n+2,m+2)} &= (1/4i)(d_{n,m}d_{n+1,m+1})
\end{aligned}$$

For the  $\Gamma_{13}$  matrix, we have

$$\begin{aligned}
\gamma_{13(n-2,m-1)} &= (1/2)(e_{n,m}a_{n-1,m-1}) \\
\gamma_{13(n-2,m+1)} &= (1/2)(c_{n,m}a_{n-1,m+1}) \\
\gamma_{13(n+2,m-1)} &= (1/2)(f_{n,m}b_{n+1,m-1}) \\
\gamma_{13(n+2,m+1)} &= (1/2)(d_{n,m}b_{n+1,m+1}) \\
\gamma_{13(n,m-1)} &= (1/2)(e_{n,m}b_{n-1,m-1} + f_{n,m}a_{n+1,m-1}) \\
\gamma_{13(n,m+1)} &= (1/2)(c_{n,m}b_{n-1,m+1} + d_{n,m}a_{n+1,m+1})
\end{aligned}$$

For the  $\Gamma_{22}$  matrix, we have

$$\begin{aligned}
\gamma_{22(n-2,m-2)} &= (1/4)(e_{n,m}e_{n-1,m-1}) \\
\gamma_{22(n-2,m)} &= (1/4)(-c_{n,m}e_{n-1,m+1} - e_{n,m}c_{n-1,m-1}) \\
\gamma_{22(n-2,m+2)} &= (1/4)(c_{n,m}c_{n-1,m+1}) \\
\gamma_{22(n,m-2)} &= (1/4)(e_{n,m}f_{n-1,m-1} + f_{n,m}e_{n+1,m-1}) \\
\gamma_{22(n,m)} &= 1 + (1/4)(-c_{n,m}f_{n-1,m+1} - d_{n,m}e_{n+1,m+1} - \\
&\quad e_{n,m}d_{n-1,m-1} - f_{n,m}c_{n+1,m-1}) \\
\gamma_{22(n,m+2)} &= (1/4)(c_{n,m}d_{n-1,m+1} + d_{n,m}c_{n+1,m+1}) \\
\gamma_{22(n+2,m-2)} &= (1/4)(-f_{n,m}f_{n+1,m-1}) \\
\gamma_{22(n+2,m)} &= (1/4)(-d_{n,m}f_{n+1,m+1} - f_{n,m}d_{n+1,m-1}) \\
\gamma_{22(n+2,m+2)} &= (1/4)(d_{n,m}d_{n+1,m+1})
\end{aligned}$$

For the  $\Gamma_{23}$  matrix, we have

$$\begin{aligned}
\gamma_{23(n-2,m-1)} &= (1/2i)(-e_{n,m}a_{n-1,m-1}) \\
\gamma_{23(n-2,m+1)} &= (1/2i)(c_{n,m}a_{n-1,m+1}) \\
\gamma_{23(n+2,m-1)} &= (1/2i)(-f_{n,m}b_{n+1,m-1}) \\
\gamma_{23(n+2,m+1)} &= (1/2i)(d_{n,m}b_{n+1,m+1}) \\
\gamma_{23(n,m-1)} &= (1/2i)(-e_{n,m}b_{n-1,m-1} - f_{n,m}a_{n+1,m-1}) \\
\gamma_{23(n,m+1)} &= (1/2i)(c_{n,m}b_{n-1,m+1} + d_{n,m}a_{n+1,m+1})
\end{aligned}$$

Finally, for the  $\Gamma_{33}$  matrix, we have

$$\begin{aligned}
\gamma_{33(n-2,m)} &= (-a_{n,m}a_{n-1,m}) \\
\gamma_{33(n+2,m)} &= 1 - (a_{n,m}b_{n-1,m} + b_{n,m}a_{n+1,m}) \\
\gamma_{33(n,m)} &= (-b_{n,m}b_{n+1,m})
\end{aligned}$$

## Appendix B

# Impact of Truncation Errors on the Capacity Calculation

<sup>1</sup> Earlier in Section 3.1.1, we had truncated our infinite-dimensional system to a finite-dimensional one. In this section we are interested in looking at the error caused due to truncation and also its effect on the capacity calculation.

We begin by restating equation (2.16) which gives the electric field due to the current density vector in terms of an integral transform, with the Green's function being the integral kernel

$$\mathbf{E}(\mathbf{r}) = \int_{V'} \mathbf{G}(\mathbf{r}, \mathbf{r}') \mathbf{J}(\mathbf{r}') dV' \quad (\text{B.1})$$

Let us call the input space  $X$  and the output space  $Y$ , i.e.  $\mathbf{J}(\mathbf{r}') \in X$  and  $\mathbf{E}(\mathbf{r}) \in Y$ .

---

<sup>1</sup>The proofs in this appendix were derived by Sandeep Krishnamurthy

Also, let us define a linear compact operator  $\mathbf{T}$  from the input space  $X$  to the output space  $Y$  such that

$$\mathbf{E}(\mathbf{r}) = \mathbf{T}\mathbf{J}(\mathbf{r}'), \quad \mathbf{T} : X \rightarrow Y \quad (\text{B.2})$$

corresponds to (B.1).

For the purpose of numerical simulations, we approximate the linear compact operator  $\mathbf{T}$  by a truncated series  $\mathbf{T}_N$ . This truncation can introduce errors in the capacity calculation. Our aim here is to determine the impact of the truncation error on the capacity calculation. To this end, we give upper and lower bounds for the capacity of the true system here, which we compare with the calculated capacity in Section 4.5 of simulation results.

*Theorem :* Let  $\sqrt{\lambda_n}$  be the  $n$ -th singular value of a linear compact operator  $A$ , then

$$\sqrt{\lambda_n(A)} = \inf_{\varphi_1, \dots, \varphi_{n-1} \in X} \sup_{\substack{\varphi \perp \varphi_1, \dots, \varphi_{n-1} \\ |\varphi|=1}} |A\varphi|$$

The spectral radius of  $A$ ,  $\sigma(A) = \sqrt{\lambda_1(A)}$ . It can be shown that for some linear compact operators  $A$  and  $B$ ,

$$\sqrt{\lambda_n(A+B)} \leq \sqrt{\lambda_n(A)} + \sqrt{\lambda_1(B)}, \quad n = 1, 2, \dots$$

Setting  $A = \mathbf{T}_N$  and  $B = \mathbf{T} - \mathbf{T}_N$ , we get the inequality

$$\sqrt{\lambda_n(\mathbf{T})} \leq \sqrt{\lambda_n(\mathbf{T}_N)} + \sqrt{\lambda_1(\mathbf{T} - \mathbf{T}_N)}$$

Setting,  $A = \mathbf{T}$  and  $B = -(\mathbf{T} - \mathbf{T}_N)$ , we get the inequality

$$\sqrt{\lambda_n(\mathbf{T}_N)} - \sqrt{\lambda_1(\mathbf{T} - \mathbf{T}_N)} \leq \sqrt{\lambda_n(\mathbf{T})}$$

Combining the two inequalities above, we get

$$\sqrt{\lambda_n(\mathbf{T}_N)} - \sigma(\mathbf{T} - \mathbf{T}_N) \leq \sqrt{\lambda_n(\mathbf{T})} \leq \sqrt{\lambda_n(\mathbf{T}_N)} + \sigma(\mathbf{T} - \mathbf{T}_N), \quad n = 1, \dots, N$$

It can be easily shown that the capacity of the true system can be upper and lower bounded by two systems defined by the eigenvalue sets (eigenvalues written in decreasing order)

$$S_1 \equiv \left\{ \left( \sqrt{\lambda_1^N} - \sigma_N \right)^2, \dots, \left( \sqrt{\lambda_N^N} - \sigma_N \right)^2, 0, 0, \dots \right\} \quad (\text{B.3})$$

and

$$S_2 \equiv \left\{ \left( \sqrt{\lambda_1^N} + \sigma_N \right)^2, \dots, \left( \sqrt{\lambda_N^N} + \sigma_N \right)^2, (\sigma_N)^2, (\sigma_N)^2, \dots \right\} \quad (\text{B.4})$$

where  $\sqrt{\lambda_1^N}, \dots, \sqrt{\lambda_N^N}$  are the  $N$  eigenvalues of  $\mathbf{T}_N$  and  $\sigma_N = \sigma(\mathbf{T} - \mathbf{T}_N)$ .

Let  $S_0 \equiv \{\lambda_1, \dots, \lambda_n, \dots\}$  be the set of eigenvalues corresponding to  $\mathbf{T}$ . Then, we have the following capacity inequality

$$C(S_1; P) \leq C(S_0; P) \leq C(S_2; P) \quad (\text{B.5})$$

where  $C(S_1; P)$  is the capacity of the system corresponding to the eigenvalue set  $S_1$  and having a total average power of  $P$  available at the transmitter.  $C(S_0; P)$  and  $C(S_2; P)$  are described similarly. In Section 4.5, we plot these capacity upper and

lower bounds along with the calculated capacity for the truncated system to demonstrate the accuracy of capacity calculations for a system truncated to a sufficiently large length.

Next, we consider the spectral radius of  $\mathbf{T} - \mathbf{T}_N$  denoted by  $\sigma_N$  and show that it goes to zero as the truncation length  $N$  goes to  $\infty$ .

$$\begin{aligned}\sigma(\mathbf{T} - \mathbf{T}_N) &= \sqrt{\lambda_1(\mathbf{T} - \mathbf{T}_N)} \\ &= \sup_{|\mathbf{J}(\mathbf{r}')| \leq 1} |(\mathbf{T} - \mathbf{T}_N)\mathbf{J}(\mathbf{r}')|\end{aligned}$$

If we define,  $\xi_n = (\int_0^a j_n^2(k_0 r') r'^2 dr')^{1/2}$  and  $\psi_{n,m}(r', \theta', \varphi') = j_n(k_0 r') Y_{n,m}(\theta', \varphi') / \xi_n$ , we can then write the vector  $\mathbf{J}(\mathbf{r}')$  in terms of the orthonormal basis set  $\psi_{n,m}(r', \theta', \varphi')$  as

$$\mathbf{J}(\mathbf{r}') = \sum_{n'=0}^{\infty} \sum_{m=-n'}^{n'} \mathbf{c}_{n',m'} \psi_{n',m'}(r', \theta', \varphi')$$

Now, using a similar analysis as we did in 3.1.1, we can write  $(\mathbf{T} - \mathbf{T}_N)\mathbf{J}(\mathbf{r}')$  as

$$\begin{aligned}(\mathbf{T} - \mathbf{T}_N)\mathbf{J}(\mathbf{r}') &= \int_{V'} [\mathbf{G}(\mathbf{r}, \mathbf{r}') - \mathbf{G}_N(\mathbf{r}, \mathbf{r}')] \mathbf{J}(\mathbf{r}') dV' \\ &= (\mathbf{I} - \hat{\mathbf{r}}\hat{\mathbf{r}}^\dagger) 4\pi k_1 \sum_{n=N+1}^{\infty} \sum_m \xi_n \mathbf{c}_{n,m} Y_{n,m}(\theta, \varphi)\end{aligned}$$

Using the orthonormal relations of the basis set and the fact that  $|(\mathbf{I} - \hat{\mathbf{r}}\hat{\mathbf{r}}^\dagger)| \leq 1$ , we can get the following upper bound on the spectral radius

$$\sup_{|\mathbf{J}(\mathbf{r}')| \leq 1} |(\mathbf{T} - \mathbf{T}_N)\mathbf{J}(\mathbf{r}')| \leq 4\pi k_1 \left[ \sum_{n=N+1}^{\infty} \sum_m \xi_n^2 |\mathbf{c}_{n,m}^2| \right]^{1/2}$$

It has been shown in [25] that

$$\xi_n^2 = \frac{\pi^2 a^2 k_0^3}{2} J_{n+3/2}^2(k_0 a) \quad (\text{B.6})$$

Using (B.6) and the facts that  $\xi_{N+1}^2$  is the largest term and  $\sum_{n=N+1}^{\infty} \sum_m |\mathbf{c}_{n,m}^2| \leq 1$ , the upper bound for the spectral radius becomes

$$\begin{aligned}
\sigma(\mathbf{T} - \mathbf{T}_N) &\leq 4\pi k_1 \xi_{N+1} \\
&= \frac{4\pi^2 k_1 k_0^{3/2} a}{\sqrt{2}} J_{N+5/2}(k_0 a) \\
&\leq \frac{\pi^{3/2} k_1 k_0^{3/2} (k_0 a)^{N+5/2}}{2^{N+3/2} (N+5/2)^{N+3} e^{-N+5/2}} \tag{B.7}
\end{aligned}$$

where we have also used the inequalities  $J_n(r) \leq |r|^n / (2^n \Gamma(n+1))$  and  $\Gamma(n+1) \geq \sqrt{2\pi n} (n/e)^n$ . For large  $N$ , we can make the right hand side of (B.7) as small as we please. Therefore, we have shown that  $\lim_{N \rightarrow \infty} \sigma(\mathbf{T} - \mathbf{T}_N) \rightarrow 0$ .

# Bibliography

- [1] C. E. Shannon, "A mathematical theory of communications," *Bell System Technical Journal*, vol. 27, pp. 379-423, Jul. 1948.
- [2] I. E. Telatar, "Capacity of Multi-Antenna Gaussian Channels", *European Trans. on Telecom. ETT*, Vol. 10, pp. 585-596, Nov. 1999
- [3] G. J. Foschini and M. J. Gans, "On Limits of Wireless Communications in a Fading Environment when using Multiple Antennas," *Wireless Personal Communications*, vol. 6, no. 3, pp. 311-335, Mar 1998
- [4] G. J. Foschini, "Layered space-time architecture for wireless communication in a fading environment when using multi-element antennas, *Bell Labs Tech. J.*, pp. 4159, Autumn 1996.
- [5] C. Berrou, A. Glavieux and P. Thitimajshima, "Near Shannon-limit error-correcting coding and decoding: Turbo-codes," *Proc. ICC'93* pp. 1064-1070, May. 1993.
- [6] D. Gesbert, M. Shafi, D. S. Shiu, P. Smith, and A. Naguib, "From theory to practice: An overview of MIMO space-time coded wireless systems, *IEEE J. Select. Areas Commun. Special Issue on MIMO Systems*, pt. I, vol. 21, pp. 281302, Apr. 2003.
- [7] A. J. Goldsmith, S. A. Jafar, N. Jindal, and S. Vishwanath, "Capacity Limits of MIMO Channels," *IEEE Journal on Selected Areas in Communications*, Vol. 21, No. 5, pp. 684-702, June 2003
- [8] A. S. Y. Poon, R. W. Brodesen and N. C. Tse, "Degrees of Freedom in Multiple-Antenna Channels: A Signal Space Approach," *IEEE Transactions on Information Theory*, vol. 51, no. 2, pp. 523-536, Feb. 2005.
- [9] A. S. Y. Poon, N. C. Tse and R. W. Brodesen, "Impact of Scattering on the Capacity, Diversity and Propagation Range of Multiple Antenna Channels," submitted to *Transactions on Information Theory*, April 2004, Revised: January 2005.

- [10] A. S. Y. Poon, R. W. Brodesen and N. C. Tse, "Spatial channel models for multiple-antenna Systems," *Proc. IEEE International Symposium on Antennas and Propagation*, June 2004 (invited paper).
- [11] T. S. Pollock, T. D. Abhayapala, and R. A. Kennedy, "Antenna saturation effects on MIMO capacity," *Proc. IEEE Int. Conf. Communications*, vol. 3, Anchorage, AK, May 2003, pp. 23012305.
- [12] T. S. Pollock, T. D. Abhayapala, and R. A. Kennedy, "Introducing space into MIMO capacity calculations," *J. Telecommun. Syst.*, vol. 242, pp. 415436, 2003.
- [13] L. W. Hanlen and M. Fu, "Wireless communications systems with spatial diversity: A volumetric approach," *Proc. IEEE Int. Conf. Communications*, vol. 4, Anchorage, AK, May 2003, pp. 26732677.
- [14] A. Paulraj, R. Nabar and D. Gore, "*Introduction to Space-Time Wireless Communications*," Cambridge University Press, Cambridge, U.K., 2003.
- [15] T. M. Cover, J. A. Thomas, "*Elements of Information Theory*," John Wiley and Sons, Inc., Canada, 1991.
- [16] R. G. Gallager, "*Information Theory and Reliable Communication*," New York: Wiley, 1968.
- [17] T. Hansen and A. D. Yaghjian, "*Plane-Wave theory of Time-Domain Fields*," IEEE Press, 1999.
- [18] R. Kress, "*Linear Integral Equations*," Springer-Verlag, AMS 82, 1999.
- [19] Z. X. Wang and D. R. Guo, "*Special Functions*," World Scientific, 1989.
- [20] J. D. Jackson, "*Classical Electrodynamics*," John Wiley & Sons, Inc., 1999.
- [21] J. D. Kraus and R. J. Marhefka, "*Antennas*," 3rd ed. NewYork: McGraw-Hill, 2001.
- [22] G. Raleigh and J. M. Cioffi, "Spatio-Temporal Coding for Wireless Communications," in *Proc. IEEE GLOBECOM'96*, pp. 18091814, 1996.
- [23] G. G. Raleigh and J. M. Cioffi, "Spatio-Temporal Coding for Wireless Communications," *IEEE Trans. Commun.*, vol. 46, pp. 357366, Mar. 1998.
- [24] B. L. Hughes, "Differential SpaceTime Modulation," *IEEE Trans. Inform. Theory*, vol. 46, pp. 145149, Nov. 2000.

- [25] S. H. Krishnamurthy, “Fundamental Limits and Joint Design of Wireless Systems with Vector Antennas ,” *PhD Dissertation*, North Carolina State University, Raleigh, Aug. 2005
- [26] C. M. James, “Adaptive Transmission Using Channel Inversion for Multiple-Antenna Systems,” *Masters Thesis*, North Carolina State University, Raleigh, Dec. 2004